KARMA

Karst **A**quifer **R**esources availability and quality in the **M**editerranean **A**rea

Report of typology of the karst systems

Deliverable 4.1

Authors:

Guillaume Cinkus (UM), Naomi Mazzilli (AU), Hervé Jourde (UM)

Date: October 2020

This project has received funding from the European Union's PRIMA research and innovation programme

Technical References

Project Acronym	**KARMA**
EU Programme, Call and Topic	PRIMA, Multi-topic 2018, Water resources availability and quality within catchments and aquifers
Project Title	Karst Aquifer Resources availability and quality in the Mediterranean Area
Project Coordinator	Prof. Dr. Nico Goldscheider, Karlsruhe Institute of Technology (KIT), nico.goldscheider@kit.edu
Project Duration	September 2019 - August 2022
Deliverable No., Name	D4.1 Report of typology of the karst systems
Dissemination Level*	Public (PU)
Work Package	WP4: Modelling Tools
Task	Task 4.1 Typology of karst hydrodynamic responses
Lead beneficiary	University of Montpellier (UM)
Contributing beneficiary/ies	Karlsruhe Institute of Technology (KIT), University of Malaga (UMA), Sapienza University of Rome (URO), Ecole nationale d'Ingenieurs de Tunis (ENIT), American University of Beirut (AUB).
Due Date	Month 12
Actual Submission Date	

* PU = public

CO = Confidential, only for members of the consortium (including the Commission Services)

RE = Restricted to a group specified by the consortium (including the Commission Services)

Version History

Version	Date
1.0	October 2020

Project Partners

(Coordinator)

Participant No *	Organisation	Country
1 (**Coordinator)**	Karlsruhe Institute of Technology (KIT)	Germany
2 **Partner 1**	Federal Institute for Geosciences and Natural Resources (BGR)	Germany
3 **Partner 2**	University of Malaga (UMA)	Spain
4 **Partner 3**	University of Montpellier (UM)	France
5 **Partner 4**	University of Rome (URO)	Italy
6 **Partner 5**	American University of Beirut (AUB)	Lebanon
7 **Partner 6**	Ecole National d'Ingénieurs de Tunis (ENIT)	Tunisia

Executive Summary

10% of the world's population is dependent on karst water resources for drinking water. Understanding the functioning of these complex, heterogeneous systems is, therefore, a major water resource management challenge. Over the past century, many methods have been developed to analyse hydrological series, and subsequently used to characterize the functioning of karst hydrosystems. These methods are a first step in the development of a conceptual model of the functioning of the studied hydrosystems, and the design of models for sustainable water resource management. However, progress in analytical tools and communication requires to reconsider classifications of hydrodynamic responses that were developed several decades ago.

WP4 proposes new approaches to the characterization and hydrodynamic modelling of karst systems, based on conceptual models, neural networks, and physical models. The first step is to propose a typology of the hydrodynamic responses of diverse karst systems, based on the analysis of discharge series measured at system outlets.

This document addresses Task 4.1 (Typology of karst hydrodynamic responses). The aim is to identify and understand the principal processes that dominate the overall behaviour of karst systems, in order to better constrain models that simulate the hydrodynamics of these hydrosystems.

The overall goal of this task was to develop a classification of karst systems and karst spring hydrodynamic responses. This requires the identification of the functioning of the various compartments within a system, and their ability to attenuate the precipitation signal, and to store and release infiltrated water. The objectives of this work are to assess the "state-of-the-art" methods used to characterize systems on the basis of their hydrodynamic response analysis, and then to examine how these methods could be updated. Opportunities for innovation in the form of new methods and the application of existing tools are also discussed.

For this task, the KARMA data were not used due to COVID-19, which induced a delayed project start of some partners. In order to keep the deadline for this deliverable, a relevant dataset of 10 karst systems was used instead, thus synergizing with the SNO KARST project (Jourde et al., 2018), the Parc Naturel Régional des Grands Causses, Suez, and the DREAL of Bourgogne Franche-Comté. In a second phase, the WoKaS database (Olarinoye et al., 2020) has been used for validating the results of the typology. The same concept can be applied to all KARMA test sites and will be done later on (either in an updated version of this deliverable, or in another suitable form), as soon as all the data are available from KARMA partners.

Table of Content

Introduction

KARMA (Karst Aquifer Resources availability and quality in the Mediterranean Area) is a European project that aims to achieve substantial progress with respect to the hydrogeological understanding and sustainable management of Mediterranean karst water resources at various temporal and spatial scales.

The main objective of WP4 is to propose a generic classification method that can be used on a maximum number of karst systems. This implies: (*i*) that it should be applicable to catchments with recent instrumentation (discharge time series over a few hydrological cycles only); and (*ii*) that it should be understandable and accessible, offering a clear and intuitive user interface. This work aims to re-evaluate existing typological approaches, based on the following questions:

- Can existing approaches be simplified or improved (through the integration of complementary indicators, improvements to methods, or the use of simple statistical indicators)?
- Is it possible to develop a systematic methodology that can be applied to a wide variety of systems?

Establishing a typology requires careful consideration of what to define and what to highlight. The information provided by a spring discharge series relates to, essentially, the inertia of the system, the degree of karstification, the estimation of reserves, and the identification of specific behaviors. The application of analyses to periods of high and low water makes it possible to highlight potential seasonal variability. However, adapting our systematic methodology to relatively short spring discharge time series makes it more difficult to characterize interannual variability (i.e. system stability), as the latter require a long period of observation.

This report is divided into five main sections:

- Section 1 presents the dataset and the karst hydrosystems analyzed in the study;
- Section 2 presents the state-of-the-art methods for analyzing spring discharge series, and presents indicators used to characterize karst hydrosystems;
- Section 3 develops the methodology and presents the results of the application of the methods to the dataset;
- Section 4 proposes a typology based on the results obtained, together with a classification methodology;
- Section 5 presents perspectives of further improvements of the proposed typology.

1 Sample data

1.1 Data selection criteria

This study aims to propose a typology of karst hydrosystems, based on the analysis of hydrodynamic series. Given this objective, it is all the more important to ensure the quality of the dataset and its relevance to the problem. Therefore, a number of karst systems were selected based on the criteria listed below, with the goal of developing a coherent dataset:

- **Hydrodynamic monitoring**: Hydrodynamic records are characterized by their quality, and the length of the time series. The confidence that can be placed in the results is directly linked to the quality and the length of the series. Quality is a function of the time step, instrumentation, and measurement uncertainty, and has a direct influence on the results of the analyses. The length of the series can also influence results as, if the observation period is too short, it creates a bias linked to meteorological conditions (e.g. a dry year). This criterion was applied to eliminate systems for which the dataset risked introducing excessive bias into the results;
- **Various hydrological functioning**: Systems were selected on the basis of several characteristics: the catchment area, mean rainfall, degree of karstification, and hydrological functioning. The objective was to study systems that cover a wide range of hydrological functioning, and thus to introduce some variety into the results;
- **Knowledge of systems**: Prior knowledge of systems hydrodynamic behavior makes it possible to ensure that results are coherent. This criterion allows selecting systems that have been the subject of comprehensive studies based on a variety of methods such as geology, cartography, field observations, tracing, geochemistry, and modeling.

1.2 The dataset

Ten karst systems, located in France, were selected (Figure 1). Data were retrieved from several organizations: the Service National d'Observation du Karst - SNO KARST (Jourde et al., 2018), the Parc Naturel Régional des Grands Causses (PNRGC), Suez, and the DREAL of Bourgogne Franche-Comté.

The characteristics of the studied systems are presented in Table 1.

Table 1: Summary of the springs studied (Thiéry, 2018; Lorette et al., 2018).

System	Station code	Mean interannual discharge m^3/s	Altitude of the spring m	Area of the catchment km^2
Aliou (La Gouarègue at Cazavet)	O0525010	0.45	441	12
Baget (Le Lachein at Balaguères)	O0485110	0.48	481	13
Durzon (The Mas de Pomier stream at Nant)	O3335010	1.46	515	117
Esperelle (The Espérelle stream at Roque-Sainte-Marguerite)	O3395010	1.17	390	91
Fontaine-de-Nîmes (Nîmes)	/	0.83	30	45
Fontaine-de-Vaucluse (La Sorgue at Fontaine-de-Vaucluse)	V6155010	17.54	105	1115
Lods (The Grand-Bief spring at Lods)	/	1.08	360	35
Mouline (The *ru* of the Mo fish farm at Lapanouse-de-Cernon)	O3416810	0.53	510	32
Mouthe (The Doubs at Mouthe)	U2002010	1.63	945	50
Toulon (The Toulon spring at Périgueux)	/	0.48	83.5	100

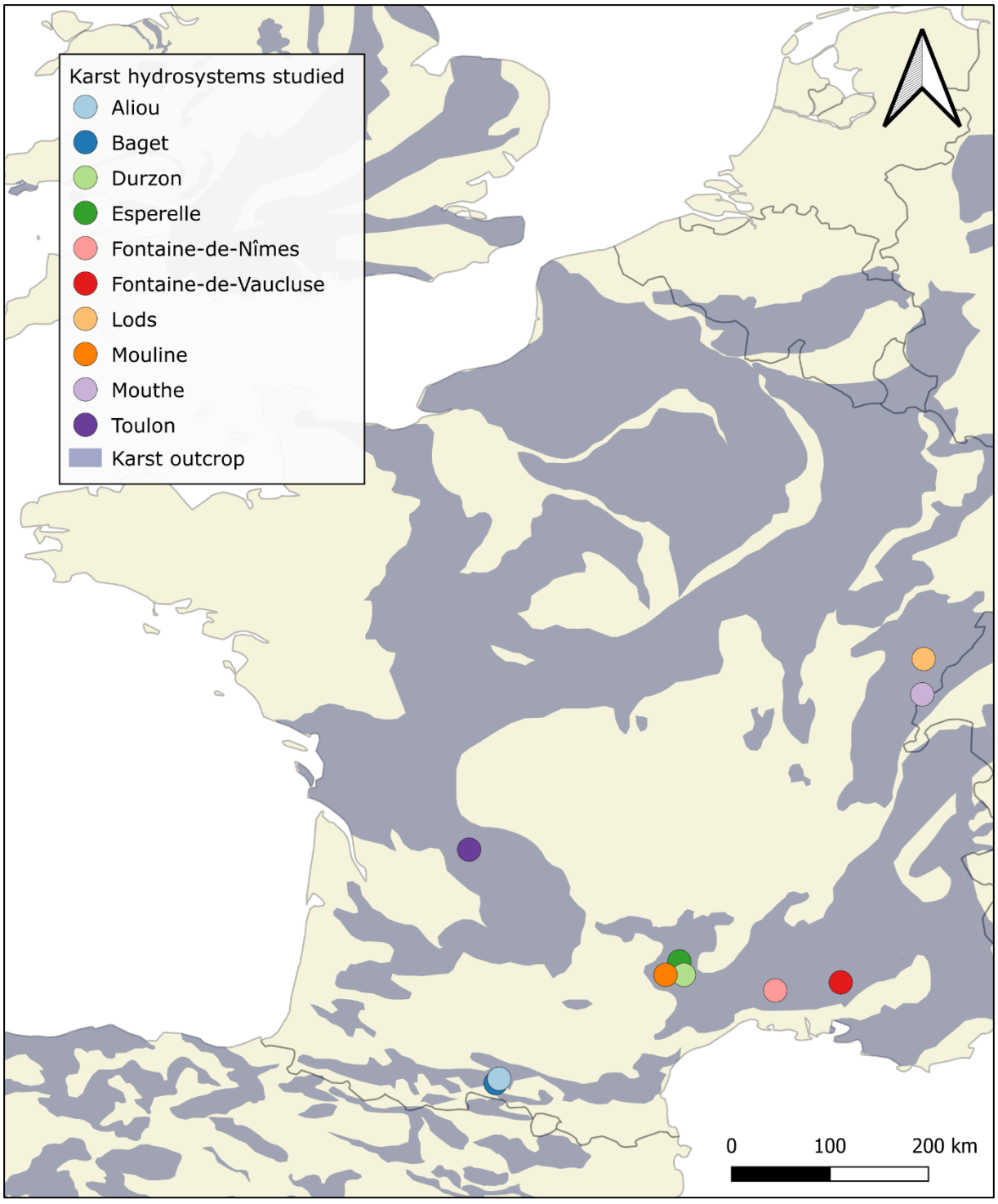

Figure 1: Location of the selected 10 karst hydrosystems.

1.3 The WoKaS database

The WoKaS database aims to improve access to data about karst systems, support large-scale comparative research, improve hydrosystem management, and promote international and interdisciplinary collaborations (Olarinoye et al. 2020). It provides details of over 400 karst systems in around 30 countries worldwide. To assess data accuracy and quality, five classes have been defined, based on four criteria. Only systems with very good quality (Class A) flow data, which met the four criteria given in Section 1.1, were included in our assessment of the proposed typology.

2 State-of-the-art of flow time series analysis methods

The analysis of flow time series at the outlet of systems is widely used to characterize the functioning of karst systems. Consequently, we developed an inventory of flow time series analysis methods with the aim of identifying those suited to the development of a typology, as follows:

- Statistical analyses,
- Analysis of recession,
- Correlational and spectral analyses,
- Analysis of classified spring discharges.

Because this study aimed to propose a way to characterize karst systems based on short time series, signal analysis methods such as wavelet or R/S analyses were not considered as they require multi-annual series.

A comprehensive, detailed review of current flow analysis methods is given in Cinkus (2020).

2.1 Statistical analyses

Basic statistical analyses of a flow time series make it possible to obtain indicators that characterize the overall functioning of a system. The most common are the mean, standard deviation, and the various quantiles. The amplitude and frequency of change in the spring discharge are a function of the system geometry, and its hydrodynamic properties (Malík, 2015).

The mean and standard deviation provide information on the size and dynamics of a system. To facilitate comparison among systems, Flora (2004) and Springer et al. (2004) proposed the **coefficient of variation** (COV):

$$COV = \frac{\sigma}{\bar{x}} * 100 \quad (1)$$

where *σ is* the standard deviation and x̄ is the arithmetic mean of a flow time series. This indicator makes it possible to dispense with the size of the system. Flora (2004) and Springer et al. (2004) have established a classification of springs based on the COV (Table 2).

The **spring variability coefficient** (SVC) is based on the comparison of discharges and the 10% and 90% quantiles:

$$SVC = \frac{Q_{10}}{Q_{90}}$$

$$4 \quad (2)$$

where *Q10* corresponds to the discharge that is exceeded 10% of the time, and *Q90* is the rate that is exceeded 90% of the time. A classification of springs is proposed by Flora (2004) and Springer et al. (2004) based on the work of Meinzer (1923), Netopil (1971) and Alfaro and Wallace (1994) (Table 3). This indicator makes it possible to ignore variability linked to extreme values.

Table 2: Classification of springs based on the flow coefficient of variation (COV) (Flora, 2004; Springer et al., 2004).

Spring's classification	Spring coefficient of variation parameter (SCVP)
Low	0 – 49
Moderate	50 – 99
High	100 – 199
Very High	> 200

Table 3: Classification of springs based on the coefficient of variability (SCV) (Flora, 2004; Springer et al., 2004).

Spring's classification	Spring variability coefficient (SVC)
Steady	1 – 2.5
Well balanced	2.6 – 5
Balanced	5.1 – 7.5
Unbalanced	7.6 – 10
Highly unsteady	>10
Ephemeral	∞

2.2 Recession analysis

The hydrograph of a flood recession corresponds to the period when discharge gradually decreases as water is not replenished (Toebes and Strang, 1964). It is possible to distinguish two regimes: (*i*) the influenced (quickflow) regime, which corresponds to the period when flow is influenced by the rapid infiltration of water into conduits in the unsaturated zone (Moussu, 2011); and (*ii*) the non-influenced (baseflow) regime, which begins when rapid infiltration ends, and corresponds to the emptying of the saturated zone and less transmissive compartments of the system. The analysis of recession is mainly used: to assess reserves (Drogue, 1972; Forkasiewicz and Paloc, 1967; Mangin, 1975); determine several indicators of the hydrodynamic functioning of the aquifer (Mangin, 1975); and provide information on flows, drainage, and the degree of karstification (Drogue, 1972; Mangin, 1975; Kullman, 2000; Malik, 2006; Kresic, 2007; Malík and Vojtková, 2012).

Our review of the literature on recession analysis identified a number of models (Boussinesq, 1878; Maillet, 1905; Horton, 1933; Barnes, 1939; Forkasiewicz and Paloc, 1967; Coutagne, 1949; Padilla et al., 1994; Mangin, 1970; Drogue, 1972; Malík and Vojtková, 2012). Initially, the objective was to identify one or more models adapted to karst hydrosystems, and to confirm or invalidate their suitability for developing a typology. The assessment focused on:

- The versatility of the model, i.e. its ability to perform well in a variety of contexts;
- The problem of equifinality, corresponding to the identifiability of parameters. Ideally, the model should have unique parameters for each type of curve. If this is not the case, it is necessary to try to obtain unique indicators on the basis of equivalent sets of parameters.

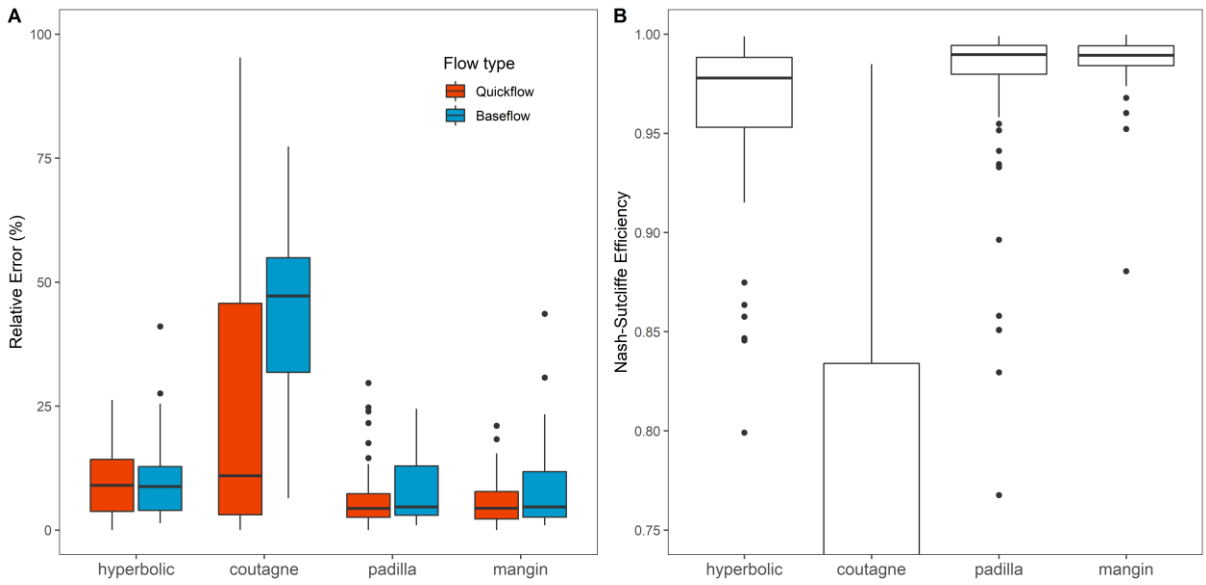

Figure 2: (A) Boxplot of errors relative to the different models for influenced and non-influenced flow regimes with respect to the observed discharge for all recessions. (B) Boxplot of Nash criteria resulting from the calibration of models over all observed recessions.

An initial review identified four models that met the project's requirements (Appendix A). All four were then tested and distinguished using dataset recessions (Appendix B), by examining their performance (Figure 2) and using sensitivity analyses (Appendix C). Three were found to be relatively successful, and relevant to the characterization of a system: the hyperbolic model (Drogue, 1972), the Padilla model (Padilla et al., 1994), and the Mangin model (Mangin, 1970). Several other avenues of research were also explored, including the development of a new model for the analysis of recession curves (see Section 5.2).

The following indicators proposed by Mangin are widely used to characterize the functioning of karst hydrosystems:

- *k* is used to characterize the capacity of a system to store and restitute precipitation;
- *i* is used to characterize the capacity of a system to filter and attenuate the precipitation signal;
- α is used to characterize the emptying of the capacitive part of the karst system. This indicator may include flows from both saturated and unsaturated zones, where in the latter a low degree of karstification may affect the response in the non-influenced regime (Mudarra and Andreo, 2011).

The analysis of *i* values on recessions in the dataset revealed a relationship between the value of this indicator, and the saturation of the system (Appendix D). Variability in *i* can be explained by the size of water stored in the karst system at the time of the flood, by the overall organization of flows in the different compartments of the system, but also by the heterogeneity of precipitation and the size of the system. We therefore decided to take account of this variability (or lack thereof) in hydrological functioning within the typology, by including a new indicator based on the amplitude of *i*.

2.3 Correlational and spectral analyses

Correlational and spectral analyses are time series analyses that characterize a system (Larocque et al., 1998). Signal analyses, mainly developed by Jenkins and Watts (1968), Hannan (1970), Brillinger

(1975) and Box and Jenkins (1976), were applied to karst hydrology by Mangin (1984). They consist of (Massei et al., 2006):

- **Simple analyses**. The simple analysis of a signal consists of calculating its autocorrelation function and the corresponding spectrum (obtained using a Fourier transformation). The principle is to compare the signal with itself over an increasingly increasing time interval (*shift*) (Jeannin and Sauter, 1998);
- **Cross-analyses**. Cross-analyses examine the transformation of the input signal into an output signal (Padilla and Pulido-Bosch, 1995).

Karst systems have a memory that is a function of the size of the reserves, and the extent to which the aquifer shows karstification (Mangin, 1984). Each system can, thus, be characterized by its response time to a unitary impulse (rain) and its inertia.

With respect to simple analyses, Mangin (1984) defined three indicators based on correlogram and spectrum analyses:

- **The memory effect**. This is the shift k for an autocorrelation coefficient r_k of 0.2. It translates variation in discharge over time, and is directly related to system inertia (Marsaud, 1997);
- **The regulation time**. This is the inverse of the bandwidth, i.e. the maximum ordinate of the spectrum divided by the integral of the function between 0 and +∞ (equal to 2). It provides information on the duration of the influence of a unitary pulse (Larocque et al., 1998; Kovács, 2003) on the volume of reserves (Marsaud, 1997), and makes it possible to assess the overall organization of flows in the system (ducts, fractures, and cracks) (Jeannin and Sauter, 1998);
- **The cut-off frequency**. This corresponds to the frequency f at which the value of the spectrum s_f becomes negligible. Beyond this frequency, the spectrum is equal to zero, and can be assimilated to noise (Jeannin and Sauter, 1998). The cut-off frequency provides information on the ability of the system to filter unitary pulses (Marsaud, 1997).

This method is based on the whole flow time series. Consequently, the results have global scope, and allow the interpretation of overall system flows. The indicators proposed by Mangin (1984) summarize the global functioning of a system, and take into account several aspects:

- The inertia of the system and its capacity to filter precipitation;
- The overall organization of flows in the system;
- The importance of water reserves.

Although this analysis provides a general idea of how a system works, it cannot highlight particular characteristics since it is based on the entire series.

Finally, the *regulation time* (which is correlated with the *memory effect*) was considered for inclusion in the typology. This is a relevant indicator to characterize the overall inertia of a system, as it takes into account the whole series, and is based on the discharge autocorrelation function.

2.4 Analysis of classified spring discharges

The analysis of classified spring discharges provides information on flow regimes within a system, based on discharge measures at the outlet (Marsaud, 1997). The analysis consists of representing the spring discharge as a function of the percentage of time it is exceeded (Malík, 2015). The method makes it possible to identify particular events inherent in karst hydrology, i.e. an overflow, leakage to another system, storage and emptying phenomena, the presence of a fluctuating impluvium and,

potentially, the ability to check the quality of the gauging station (Grasso and Jeannin, 1994; Marsaud, 1997; Dörfliger, 2010).

Table 4: Interpretation of the inflexion point for classified spring discharges, showing low and high percentage (or both) inflexion points. The numbering of α follows the discharge axis, i.e. from left to right.

Case	Slope of the line	Location of the inflexion point	Interpretation
A	α1 < α2	High percentages	- Overflow - Leak to another system - Temporary storage - Leakage or overflow of the gauging station during high waters
B	α1 > α2		- Contributions from another system - During floods, the gauging station takes into account flows that do not belong to the system.
C	α1 > α2	Low percentages	- Contribution of a reserve from an earlier cycle
D	α1 < α2		- Constitution of a reserve
E	α1 < α2 α2 > α3	Dual change	- Trapping of a reserve as water recedes, and restitution during drying up

Drawing on empirical observations, Mangin (1971) suggested that the distribution of discharge from karst springs or their logarithm can be approximated by a half-normal Gaussian distribution. He concluded that the comparison of quantiles for measured spring discharges with quantiles given by this reference distribution should follow a straight line. According to this theory, any anomalies indicate inhomogeneity in the operation of the system, below or above a certain range of discharge. The interpretation proposed by Mangin is based on an extremely strong hypothesis, which is that the statistical distribution represents reality.

The interpretation is based on the identification of discontinuities or anomalies, corresponding to an inflexion point for classified spring discharges. Such changes can occur at low or high discharges, and may be positive or negative (Table 4).

This method provides information that complements that supplied by other methods and was, therefore, considered for the identification of specific system functions (e.g. the activation of an overflow outlet).

3 Application of the methods to the dataset

3.1 Statistical analyses

Statistical indicators provide an initial assessment of the functioning of a system. The following indicators are considered relevant in characterizing a karst system:

- **Mean interannual discharge**, which is a function of the size of the catchment and mean precipitation;
- The **COV**, which is a scaled indicator that allows systems to be compared on the basis of their general flow dynamics;
- **Observed minimum and maximum discharges**, which make it possible to understand the flow amplitude. However, significant uncertainty is associated with this indicator, due to uncertainty relating to the extrapolation of extreme discharges;
- **SVC** is a scaled indicator that provides information on flow variability, and is less biased by extreme values;

- The **specific discharge** makes it possible to take the dimensions of the system into consideration. This indicator requires knowledge of the size of the catchment. It is, therefore, not always available and is dependent on the quality of hydrogeological studies.

It is most suitable to use scaled indicators, such as the COV, the SVC, and the specific discharge, when comparing systems. However, the mean interannual discharge may be needed to assess certain characteristics of hydrodynamic functioning.

The results of the selected statistical indicators are presented in Table 5.

Table 5: Basic spring discharge indicators for the studied systems.

System	Mean discharge m^3/s	Coefficient of variation %	Minimum discharge m^3/s	Maximum discharge m^3/s	SVC	Specific discharge mm/j
Aliou	0.45	190.4	0	28.91	32.1	3.20
Baget	0.49	147.2	0.02	10.10	14.0	3.22
Durzon	1.63	60.7	0.69	17.80	3.3	1.20
Esperelle	1.06	147.3	0.11	23.30	11.7	1.01
Fontaine-de-Nîmes	0.54	228.0	0	18.09	40.2	1.03
Fontaine-de-Vaucluse	17.54	71.3	2.79	85	5.9	1.36
Lods	1.00	131.4	0.15	11.72	20.0	2.48
Mouline	0.51	47.8	0.19	4.67	2.6	1.36
Mouthe	1.92	125.4	0.01	19.50	25.4	3.31
Toulon	0.48	37.0	0.25	0.96	2.5	0.41

3.2 Analysis of recession curves

3.2.1 Methodology

The flow dynamics of karst systems are highly variable and mainly depend on their structure and size. A karst system can be characterized into one of two categories based on its dynamics:

- **intra-day**: the system is reactive, with rapid variation in discharge, of the order of an hour;
- **multi-day**: the system has high inertia and variation in discharge that can be measured on a daily basis.

In order to optimize resolution, the hourly time step was used where possible, but a daily time step was used when hourly time steps were not possible. The length of dataset series varied from a single decade to several decades (Table 6). Three series recorded daily data and seven recorded hourly data.

Recession curves were selected from the overall series with no consideration given to the period (seasonal or infra-annual recession), with the following conditions:

- The peak flood discharge must be high (at least one tenth of the maximum in the flow time series);
- There should be little or no disruption during the recession (i.e. precipitation leading to untimely peaks). In cases where the disruption was of short duration, data could be removed and replaced with a blank;
- The recession must be complete, in other words, it should include both the influenced regime and the entire non-influenced regime (with some tolerance for high-inertia systems).

Table 6: Details of flow time series used for the studied systems.

System	Time series dates		Time step
	Start	End	
Aliou	1970-01-10	2014-12-31	daily
Baget	1968-04-25	2015-09-29	daily
Durzon	2010-12-03	2019-11-30	hourly
Esperelle	2011-12-08	2019-11-30	hourly
Fontaine-de-Nîmes	1998-10-28	2017-08-17	hourly
Fontaine-de-Vaucluse	1966-01-02	2020-04-26	daily
Lods	2013-10-01	2020-02-20	hourly
Mouline	2010-12-09	2019-12-01	hourly
Mouthe	2013-01-01	2020-04-02	hourly
Toulon	2016-02-03	2018-08-02	hourly

In the specific case where system flow was affected by a hydrodynamic operation (e.g. the activation of an overflow outlet), and was visible on the recession curve (as an inflexion point), we selected the last, unaffected part of the curve, including the dry-off. This approach ensured that the models, which cannot take account of inflexion points, were correctly calibrated. Information loss was relatively minor, as discharges that were excluded from the analysis only represented a tiny part of the overall flow.

3.2.2 Results

The tested recession models performed well, and led to the identification of several indicators. An innovative recession model, currently under development (see Section 5.2), appears to very promising in terms of performance and system characterization. Pending finalization of this model, we recommend the use of the Mangin model, which can characterize both influenced and non-influenced regimes.

The analysis of the influenced regime provided values for *i,* which characterizes the capacity of a system to filter precipitation. Results for the studied systems (Figure 3(A)) clearly differentiate among systems, and are consistent with the values found in the literature. The amplitude of *i* values in certain systems highlights the variability in their hydrological functioning.

The analysis of the non-influenced regime provided values for *k*, which characterizes the capacity of a system to store and restitute precipitation. Again, results for the studied systems (Figure 3(B)) clearly differentiate among systems, and are consistent with values found in the literature.

The parameter α, derived from the exponential equation, characterizes the emptying of the capacitive part of the karst system (Figure 3(C)). This information is important in the development of a typology, as it can distinguish systems based on flow dynamics.

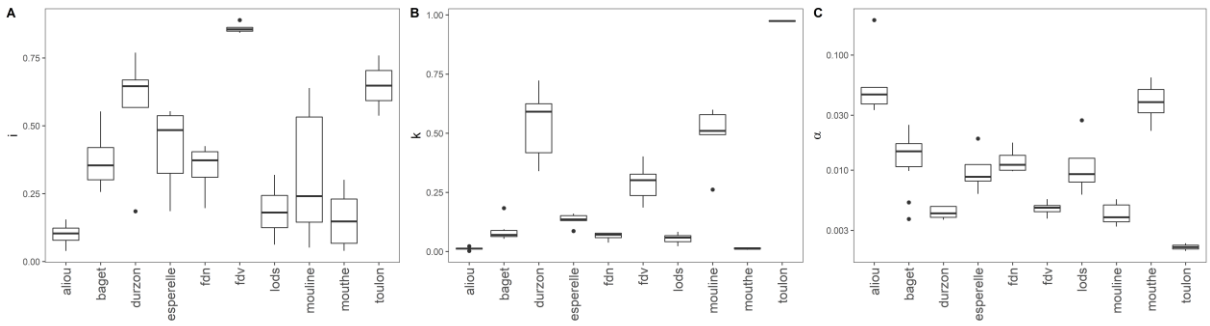

Figure 3: Results for each of the indicators proposed by Mangin (1984) using the recessions for each of the studied systems: (A) *i*, (B) *k*, and (C) *α*.

3.3 Correlational and spectral analyses

3.3.1 Methodology

Mangin (1984) defined two types of analysis:

- Short-term analyses, with a sampling step of 1 day and a maximum offset *m* of 125 days (~ *n/3* with *n* = 365);
- Long-term analyses, with a sampling interval of 10 days and a maximum offset *m of* 1250 days.

Long-term analysis requires fairly long time series (10 years). Out of the data available for the study, only two series (out of a total of ten) and 61% of the WoKaS class A data (Olarinoye et al., 2020) complied with this condition. We therefore decided to carry out short-term analyses to enable the comparison of as many systems as possible.

As the systems included in the dataset are all subject to a similar climate, the starting date for the flow time series was set as the beginning of the hydrological cycle (1 September). This allowed the analysis to take account of seasonality.

3.3.2 Results

The results of correlational and spectral analyses highlighted the diversity of hydrological functions in the studied systems (Figure 4, Table 7). The three indicators proposed by Mangin (1984) made it possible to quantify this functioning, and it was thus possible to distinguish the following categories on the basis of our results:

- Very reactive systems, with almost no filtration capacity. These systems rapidly transmit a response that is proportional to the intensity and duration of unitary pulses (precipitation). The Aliou and Mouthe systems fall into this category, with a memory effect of under 10 days, a regulation time of under 15 days, and a cut-off frequency above 0.4 day^{-1};
- Low-inertia systems, which, although notably less reactive than those detailed above, still have fast response times. The Baget, Fontaine-de-Nîmes, and Lods systems fall into this category, with a memory effect of 10–20 days, a regulation time of 15–25 days, and a cut-off frequency of 0.3–0.4 day^{-1};
- Medium-inertia systems are able to filter a greater-or-lesser proportion of unitary pulses. This class encompasses a wide variety of behaviors, ranging from reactive to high-inertia systems. The Durzon, Esperelle, and Mouline systems fall into this category, with a memory effect of

20–50 days, a regulation time of 25–50 days, and a cut-off frequency of 0.2–0.3 day^{-1}. The Esperelle differs from the other two systems as values are towards the lower limits of the class, indicating greater reactivity;

- High-inertia systems have high filtration capacity. The Fontaine-de-Vaucluse and Toulon systems fall into this category, with a memory effect of over 50 days, a regulation time of over 50 days, and a cut-off frequency of under 0.2 day^{-1}. The high inertia of these systems may be due to low karstification, the complexity of the system architecture, or the system size. The high inertia of the Fontaine-Vaucluse system can be explained by the large surface area of its catchment, estimated to be over 1000 km^2 (Blavoux et al., 1992). The Toulon system, defined as a complex by Lorette et al. (2018), is a multi-layer aquifer, with flow that is permanently supported by the confined aquifer part of the system.

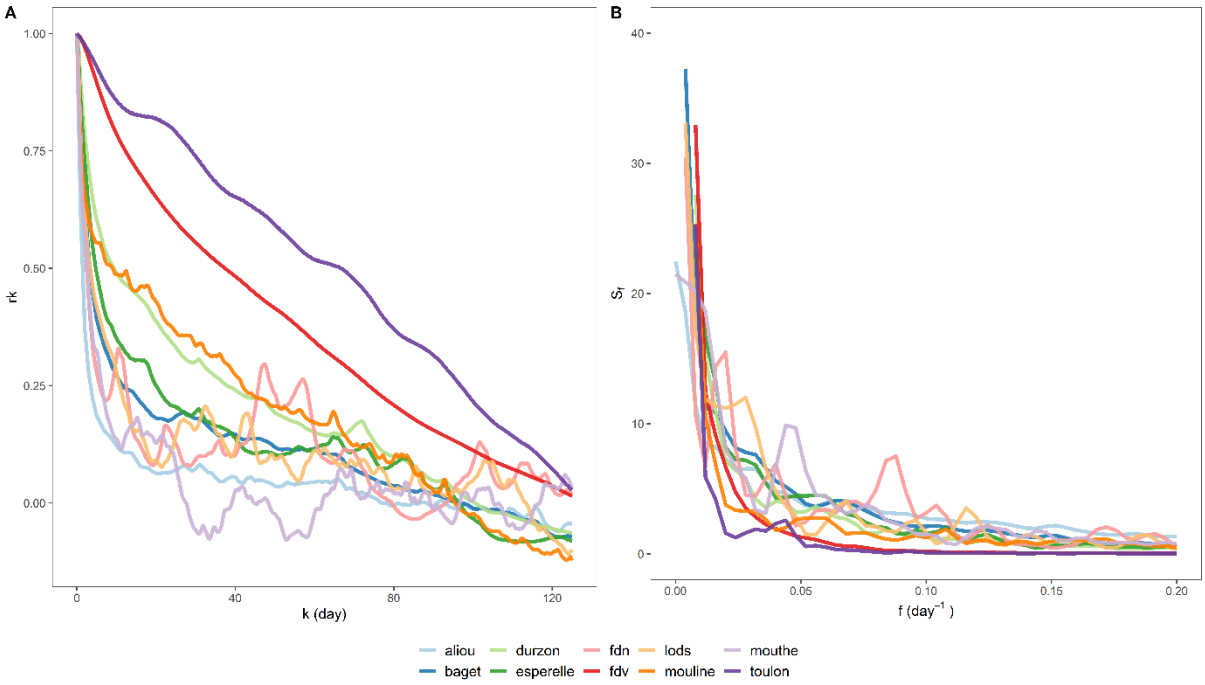

Figure 4: Autocorrelation function (A) and variance density spectrum (B) analyses of flow time series for the studied systems.

Within a category, the variability of an indicator can characterize the specific functioning of a system (especially systems with medium or high inertia), which can be explained by general knowledge of the system, such as its catchment, geology, hydrodynamic functioning, and precipitation regime.

Table 7: Results of correlational and simple spectral analyses for the studied systems.

System	Memory effect *day*	Regulation time *day*	Cut-off frequency day^{-1}
Aliou	4.6	11.2	0.41
Baget	17.6	24.4	0.34
Durzon	49.1	40.0	0.24
Esperelle	25.8	28.4	0.25
Fontaine-de-Nîmes	13.2	21.8	0.33
Fontaine-de-Vaucluse	81.4	67.8	0.13
Lods	12.6	22.1	0.36
Mouline	53.0	40.8	0.265
Mouthe	7.3	10.7	0.415
Toulon	101.7	85.8	0.08

3.4 Analysis of classified spring discharges

The analysis of classified flows characterizes specific behaviors of karst systems. The method is difficult to implement, and requires prior knowledge of the system or field observations. We propose a methodology in the form of a large-scale typology. The aim is to simplify the analysis, and use it to identify the **major**, specific behaviors that characterize each system. We believe that this interpretation complements the results of the typology, as it provides information that is considerably different from that of other analyses.

3.4.1 Methodology

Given the global nature of our work, and the large number of systems under consideration, it was not possible to confirm our interpretations with field observations. Therefore, the analysis was designed to benefit from the advantages of the method, while minimizing interpretation uncertainties. Details are given below:

- Estimates of **drought discharges** are subject to a high degree of uncertainty, which can mean that inflexion points are difficult to interpret. Moreover, the analysis lacks rigor, given the almost deterministic evolution of these discharges (Mangin, 1975). We therefore decided to filter flow time series and only retain discharges above Q90 (corresponding to the discharge that is exceeded 90% of the time);
- In the case of **flood discharges** and, more specifically, very high discharges, it is very difficult to distinguish an unusual behavior from an unreliable measurement. Therefore, it is generally better to exclude data that corresponds to ungauged discharges in order to improve the robustness of the interpretation. Therefore, we did not take into account discharges that exceeded the cumulative percentage threshold of 99.9%.

The objective was to identify the presence or absence of **major** system behaviors, and avoid any over-interpretation, and the following were differentiated (Figure 5):

- Systems with no apparent, particular behavior **(A)**;
- Systems in which the hydraulic or flow properties changed beyond a certain discharge. This interpretation is characterized by an inflexion point at low percentages, when a given slope is followed by a less steep slope **(B)**;
- Systems in which an overflow outlet is activated, there is flow to another system, or the temporary storage of water occurs above a certain discharge. This interpretation is characterized by an inflexion point at high percentages, when a given slope is followed by a steeper slope **(C)**.

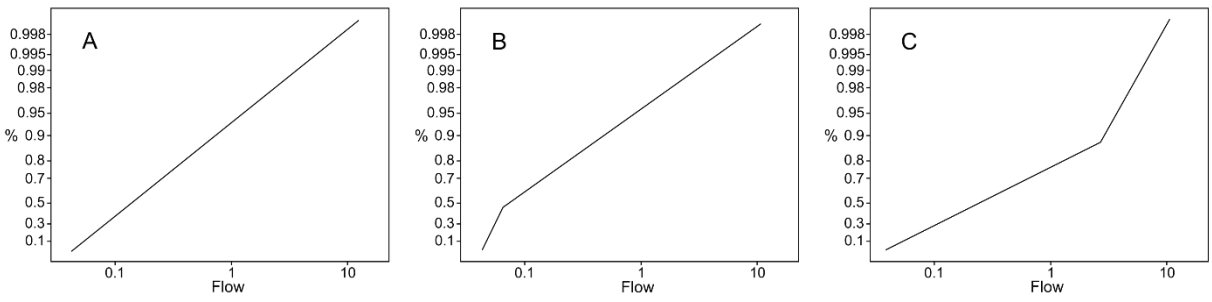

Figure 5: Proposed interpretation of the results of the classified spring discharges analysis: (A) No major specific behaviors; (B) Change in the hydraulic or flow properties of the system; and (C) Activation of an overflow outlet, flow to another system, or temporary storage of water.

3.4.2 Results

The results of the analysis are presented in Appendix E.

4 Proposal of a typology based on the selected indicators

4.1 Analysis of the dataset using hierarchical partitioning methods

The purpose of data clustering is to identify clusters that contain observations or objects with similar characteristics (Jain et al., 1999; Govender and Sivakumar, 2020). Clustering analysis can be used to identify archetypes, and offer a better understanding of the structure within a dataset (Halkidi, 2001). This technique is considered unsupervised, because it is not based on predefined classes or examples that would give an idea of the structure of the dataset (Berry and Linoff, 1996).

4.1.1 Methodology

Assessment of the dataset and selection of indicators

The selection criterion for the ten studied systems was that there should be variation in hydrological functioning to ensure a representative population. The sample contains no extreme data that could influence the results of the analysis. There was, nevertheless, an important bias linked to the sample size (n = 10), which is important to consider when interpreting the results.

Indicators were selected based on the literature review (here, the aim was to retain indicators with a particular physical meaning). A second consideration was the analysis of results for each method and principal component analyses (to identify complementary indicators and avoid duplication). The following six indicators were selected:

- Mean interannual discharge (Q_{mean}). This indicator takes into account the size of the catchment, which has an impact on the inertia of the system and its response to outflow;
- The coefficient of variation (COV). This indicator provides information on the reactivity of the system, and the distribution of its flows;
- Mean α (α_{mean}). This indicator characterizes the emptying of the capacitive part of the karst system and, by extension, its contribution to the flow;
- The maximum observed value of k (k_{max}). This indicator characterizes the maximum capacity of the system to store and release precipitation;
- The maximum observed value of i (i_{max}). This indicator characterizes the maximum capacity of the system to attenuate the precipitation signal;
- The standard deviation of i (i_{sd}). This indicator characterizes the variability of the hydrodynamic functioning of a system.

Data were centered-reduced because the means and standard deviations of indicators varied widely.

Choice of the measure of similarity or dissimilarity

The choice of the measure of dissimilarity or similarity is a function of the context of the study, the nature of the dataset, and the clustering method (Gower and Legendre, 1986). The best choice is a combination of experience, skills, knowledge, and luck (Gan et al., 2007).

As the dataset was reliable, with no extreme values and little noise, the Euclidean measure of dissimilarity (the most widely used method), was selected (Gan et al., 2007; Govender and Sivakumar, 2020). It has been found to be appropriate for data with no extreme values and the average measure of dissimilarity has been shown to be most effective for 'simple' and 'average' distance hierarchical partitioning methods (Shirkhorshidi et al., 2015). In our study, the final result of testing was identical for both the Euclidean or average dissimilarity measure.

The Euclidean distance between two points *x* and *y* of a *d*-dimensional dataset is calculated as follows (Gan et al., 2007):

$$d_{euc}(x,y) = [\sum_{j=1}^{d}(x_j - y_j)^2]^{\frac{1}{2}} = [(x-y)(x-y)^T]^{\frac{1}{2}} \quad (3)$$

where x_j and y_j are the values of the j[th] attribute of *x* and *y*, respectively.

Choice of clustering method

A good knowledge of the data and indicators relating to the karst systems can avoid the need for complex methods, and facilitate the system-specific interpretation of results. This study aimed to define a number of classes that distinguish karst systems and identify the indicators that can be used to discriminate between the different clusters. A hierarchical partitioning method was selected to associate the branches of the dendrogram with physical system characteristics. Hierarchical partitioning methods have the following advantages compared with non-hierarchical methods (Govender and Sivakumar, 2020):

- It is not necessary to know the number of clusters prior to the analysis;
- The results do not depend on the choice of initial centers (Tufféry, 2011), which is a problem with non-hierarchical partitioning methods;
- The graphical representation (dendrogram) provides an understanding of the cluster structure and how they are connected;
- The method is suitable for clusters of different sizes and shapes.

The main disadvantages are as follows:

- the long processing time;
- the difficulty of determining the number of relevant clusters after analysis (Govender and Sivakumar, 2020).

However, given the small size of our dataset, and the fact that we have good knowledge of both systems and indicators, these disadvantages do not represent a particular constraint.

There are several hierarchical partitioning methods, the most common being single-link, complete link, group average, weighted group average, Ward, centroid and median. We selected the Ward method, which is known to be effective (Milligan and Cooper, 1987), and which corresponds best to the concept of clustering (Tufféry, 2011). Our choice was confirmed by testing the different methods on the dataset and assessing the results. This showed that most of the methods were biased by the Fontaine-de-Vaucluse system, which has a high mean discharge compared with the others.

Ward's hierarchical partitioning method is as follows:

1. Each observation is considered as an initial cluster;

2. Distances between each cluster are calculated;
3. Clusters are merged. The algorithm consists of merging all possible combinations of clusters and retaining the one that minimizes inter-cluster inertia;
4. Steps 2 and 3 are repeated until only one cluster, which contains all observations, remains.

The Ward distance between two clusters *A* and *B* that have centers of gravity *a* and *b* and frequencies n_A and n_B is equal to:

$$d(A,B) = \frac{d(a,b)^2}{n_A^{-1} + n_B^{-1}} \quad (4)$$

The result of the analysis is presented in the form of a dendrogram.

4.2 Results and interpretation

Figure 6 shows the hierarchical partitioning result in the form of a dendrogram, and the interpretation of the different nodes. Firstly, systems are discriminated on the basis of their reactive or inertial nature, which includes their capacity to filter, store, and restitute rainfall. This distinction is essentially reflected by the indicators k_{max}, COV, and i_{max}. In the second step, subgroups are identified for each type of system:

- **Reactive systems**: The first node in the reactive systems branch is explained by the contribution of the capacitive part of the system to the flow. It is possible to distinguish: (*i*) systems in which the capacitive part has a weak influence, or where the contribution to the flow is weak (Aliou and Mouthe); and (*ii*) systems in which the capacitive part makes an important contribution to the flow (Fontaine-de-Nîmes, Lods, Baget, and Esperelle). Two indicators make it possible to discriminate between these two clusters: α_{mean} and i_{max}. α_{mean} characterizes the average dynamics of the emptying of the capacitive part of the system, and i_{max} has very low values in systems where the capacitive part of the system makes little contribution. Although *i* characterizes the contribution of flows linked to the influenced regime, it is indirectly affected by flows coming from the capacitive part;
- **Inertial systems**: The first node of the inertial systems branch discriminates between large systems (Fontaine-de-Vaucluse) and small or medium systems (Toulon, Mouline, Durzon). This distinction is based on Q_{mean}, which corresponds to the mean interannual discharge, and which is proportional to the size of the system;
    - **Small/medium sized inertial systems**: The second node of the inertial systems branch discriminates between small and medium-sized systems based on variation in their hydrodynamic functioning. It distinguishes stable and regular systems (Toulon) from systems in which there is variation in hydrodynamic functioning depending on the saturation of the system (Mouline, Durzon). This distinction is revealed by i_{sd}, the standard deviation of indicator *i*.

We decided to interpret the second node of the inertial systems branch (Toulon, Mouline, and Durzon), and not the second node of the reactive systems branch (Fontaine-de-Nîmes, Lods, Baget, and Esperelle), despite the fact that the latter further reduces inter-cluster inertia. This choice was justified by the physical significance of the selected nodes, and their relevance within the framework of a typology. The Class 2 cluster (Fontaine-de-Nîmes, Lods, Baget, and Esperelle) has a first node that discriminates between two groups of systems: Fontaine-de-Nîmes and Lods/Baget/Esperelle. This difference can be explained by the high coefficient of variation of Fontaine-de-Nîmes (228.0%)

compared with the others (131.4%, 147.2%, and 147.3%, respectively). This information is irrelevant in the context of the typology, as it introduces more complexity without adding any major characteristics.

Thus, the analysis made it possible to:

- Identify indicators that can differentiate karst systems: *k*, *i*, *α*, regulation time, the coefficient of variation, and the mean interannual discharge;
- Assess possible classes in the dataset. They can initially be discriminated based on their reactive or inertial character, then (*i*) as a function of the emptying of the capacitive part of the system for reactive systems, and (*ii*) as a function of the mean interannual flow and variability in hydrodynamic operation for inertial systems.

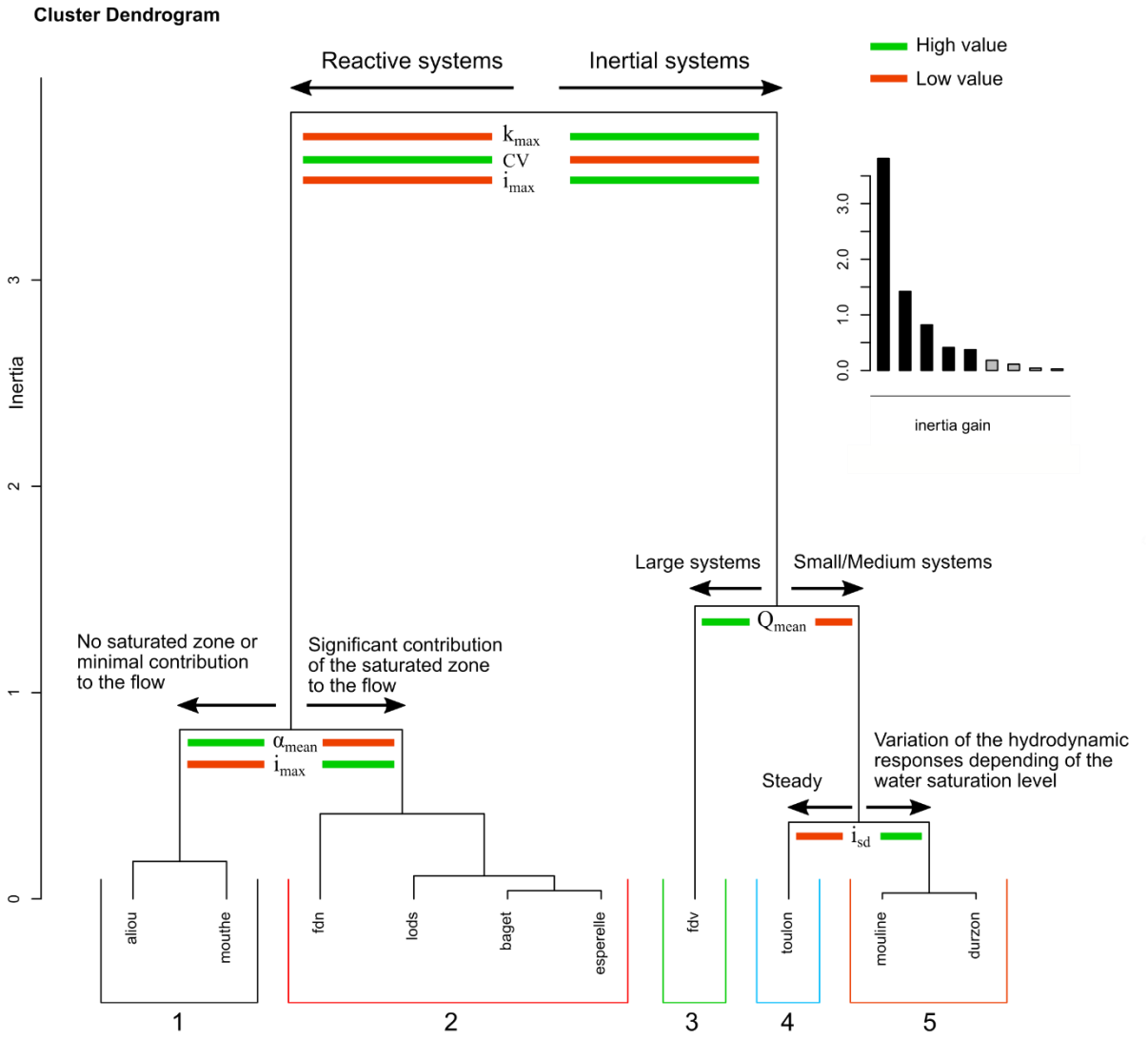

Figure 6: Hierarchical partitioning of the systems in the dataset based on the six selected indicators, showing a detailed interpretation of nodes, and the contribution of indicators to the differentiation of systems.

4.3 The proposed typology

4.3.1 Establishing the typology

Our results and tests of various indicators that could potentially differentiate the ten systems led to development of a proposed typology. It seems that the inertia of a system (its capacity to filter precipitation) is a characteristic that is independent of its capacity to store and restitute precipitation. In other words, systems with relatively high inertia can have a low or a high water-storage capacity. An exception occurs when storage capacity is high, in which case the system will necessarily be inertial. Thus, the best approach seems to be to initially differentiate systems based on their capacity to store and restitute precipitation and then, in a second step, to observe the inertial character of their hydrodynamic functioning.

Contrary to the hypothesis put forward in the context of hierarchical partitioning analysis, it does not seem relevant to use the mean interannual discharge (Q_{mean}) in the classification because this approach introduces unnecessary complexity into the typology, and considerably increases the number of classes to be defined. However, it should be noted that, for large systems, the interpretation of indicators may be biased by the size of the basin, the heterogeneity of rainfall, or the homogenization of responses.

Definition of classes

Five classes were chosen to represent the dataset and discriminate systems based on their functioning. Increasing this number did not lead to further differentiation of the remaining systems based on their major operating characteristics.

This study, thus, distinguished five main types of karst systems:

1. A class of systems with very low to low storage capacity, in which the capacitive part of the system: (*i*) is small and poorly developed; (*ii*) contributes little or nothing to run-off; or (*iii*) drains quickly. A high level of karstification allows rapid water transfer;
2. A class of systems with a low to medium storage capacity, in which the capacitive part of the system is moderately developed and empties moderately. A high level of karstification allows rapid water transfer;
3. A class of systems with a low to medium storage capacity, in which the capacitive part of the system is moderately developed and empties moderately. Low to medium karstification is consistent with a relatively homogeneous response;
4. A class of systems with moderate to high storage capacity, in which the hydrodynamic response is influenced by the saturation of the system. There is a high level of karstification, and different compartments are called upon as a function of periods of high and low water;
5. A class of systems with a moderate to high storage capacity, in which the hydrodynamic response is relatively homogeneous. These are small- to medium-size systems with little or no karstification, or large, complex systems.

Thus, the studied systems fall into the following classes:

- Class 1: Aliou, Mouthe;
- Class 2: Baget, Esperelle, Fontaine-de-Nîmes, Lods;
- Class 3: /;
- Class 4: Durzon, Mouline;

- Class 5: Fontaine-de-Vaucluse, Toulon.

Characterization of system inertia

The inertial nature of a system and its flow regime are expressed by indicators such as *i*, the regulation time, the coefficient of variation, or the SVC. The **regulation time** appears to be the best indicator to characterize overall system inertia as it considers the whole series and is based on the discharge autocorrelation function.

The analysis of our dataset highlights a very good relationship between the proposed classes and regulation time (Table 8):

- Class 1 (Aliou, Mouthe) has regulation times around 10 days;
- Class 2 (Baget, Esperelle, Fontaine-de-Nîmes, Lods) has regulation times between 20 and 30 days;
- Class 4 (Durzon, Mouline) has regulation times of about 40 days;
- Class 5 (Fontaine-de-Vaucluse, Toulon) has regulation times of more than 70 days.

For systems with low storage capacity (Classes 1, 2, and 3), regulation time is function of the contribution of the capacitive part of the system to flow and the degree of karstification. For systems with high storage capacity, it is: (*i*) low to medium for systems with highly variable hydrodynamic operation (Class 4); and (*ii*) high for stable, regular systems (Class 5).

Example: Regulation times for the four systems in Class 2 are consistent with their known reactivity. According to the literature, and the results of our analyses, it is possible to order them based on their reactivity – Fontaine-de-Nîmes, Lods, Baget, and Esperelle – with Fontaine-de-Nîmes being the most reactive system, and Esperelle the least reactive. The Fontaine-de-Nîmes, Lods, Baget, and Esperelle systems have regulation times of 21.8, 22.1, 24.4, and 28.8, respectively. This order, based on regulation time, corresponds to values reported in the literature and results from other indicators.

Thus, regulation time seems to be the best indicator to characterize the inertia of systems because it reflects the overall functioning of a system. We therefore propose that it should be used to refine the interpretation once the class has been defined.

Table 8: Values of indicators for the studied systems.

System	k_{max}	i_{min}	α_{mean}	Regulation time	Class
Aliou	0.02	0.04	0.063	11.2	1
Baget	0.18	0.26	0.014	24.4	2
Durzon	0.72	0.19	0.004	40.0	4
Esperelle	0.16	0.19	0.011	28.4	2
Fontaine-de-Nîmes	0.08	0.20	0.012	21.8	2
Fontaine-de-Vaucluse	0.4	0.84	0.005	67.8	5
Lods	0.08	0.06	0.012	22.1	2
Mouline	0.60	0.05	0.004	40.8	4
Mouthe	0.02	0.04	0.041	10.7	1
Toulon	0.98	0.54	0.002	85.8	5

4.4 Methodology for classifying a system based on indicator values

Next, we turn to the indicators that best-characterize each class. We can define the following rules:

- Classes 1, 2, and 3 are differentiated from Classes 4 and 5 by k_{max};
- Class 1 is differentiated from Classes 2 and 3 by α_{mean};
- Class 2 is differentiated from Class 3 by i_{min};
- Class 4 is differentiated from Class 5 by i_{min}.

i_{min} is preferred to i_{sd} because it is more robust, and is less biased by the number of recessions. The flowchart, presented in Figure 7, shows the methodology for classifying a karst system based on the results of the various analyses. It consists of considering values for different indicators in a logical order:

1. k_{max}: this differentiates systems with a very low to medium storage capacity (Classes 1, 2 and 3) from systems with moderate to high capacity (Classes 4 and 5);
    - If $k_{max} \leq 0.4$ the value of α_{mean}: this differentiates Class 1 from Classes 2 and 3;
        - If $\alpha_{mean} > 0.03$ the value of i_{min}: this differentiates Class 2 from Class 3;
    - If $k_{max} > 0.4$ the value of i_{min}: this differentiates Class 4 from Class 5.

Regulation time complements the classification methodology, as it provides an intra-class differentiation of systems based on the inertial character of their hydrodynamic operation. Finally, the analysis of classified spring discharges highlights the presence (or not) of a major, specific behavior.

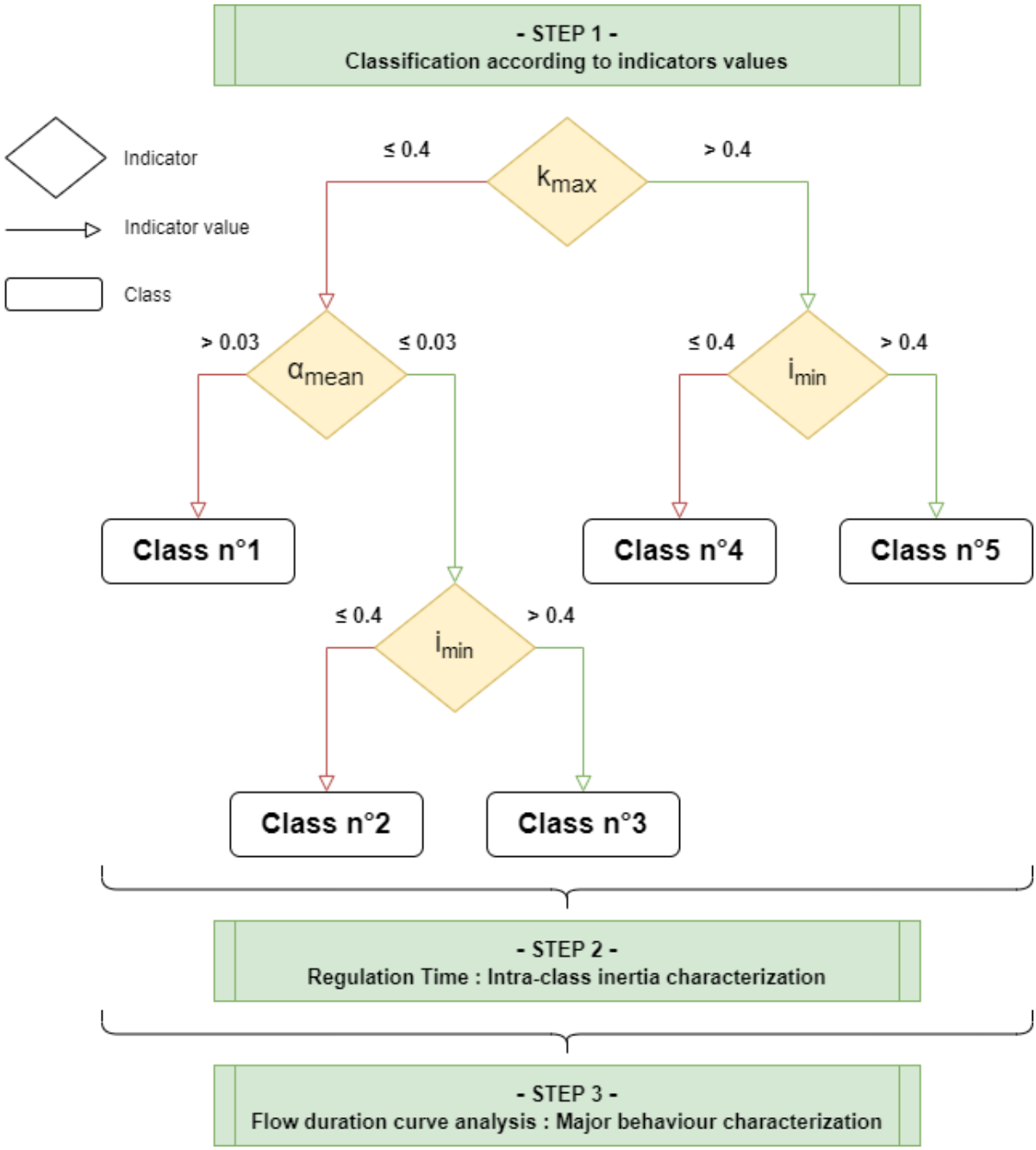

Figure 7: Diagram of the methodology for classifying a karst system based on indicators developed form analyses of flow time series.

4.5 Validation of the typology and the analysis methodology

System overview

In order to validate the methodology and the proposed classes, analyses were run on four other karst systems. Three are located in France (Cents-Fonts, Homede, and Boundoulaou), and one in Lebanon (Qachqouch).

Results

The results of the analyses, presented in Table 9, make it possible to classify the four systems on the basis of the methodology presented in Figure 7.

Table 9: Value of indicators for the studied systems.

System	k_{max}	i_{min}	α_{mean}	Regulation time	Class
Cent-Fonts	0.27	0.23	0.007	28.2	2
Qachqouch	0.15	0.08	0.034	32.5	1
Homede	0.27	0.23	0.009	37.1	2
Boundoulaou	0.34	0.20	0.009	41.0	2

The Cents-Fonts system belongs to Class 2 with $k_{max} \leq 0.4$, $\alpha_{mean} \leq 0.03$, and $i_{min} \leq 0.4$. Its regulation time of 28.2 corresponds to an average value for this class.

The Qachqouch system belongs to Class 1 with $k_{max} \leq 0.4$, and $\alpha_{mean} > 0.03$. Its regulation time of 32.5 corresponds to a high value for this class.

The Homede system belongs to Class 2 with $k_{max} \leq 0.4$, $\alpha_{mean} \leq 0.03$, and $i_{min} \leq 0.4$. Its regulation time of 37.1 corresponds to a high value for this class.

The Boundoulaou system belongs to Class 2 with $k_{max} \leq 0.4$, $\alpha_{mean} \leq 0.03$, and $i_{min} \leq 0.4$. Its regulation time of 41.0 corresponds to a high value for this class.

Thus, the Qachqouch system is classified as a system with a high level of karstification, allowing rapid water transfer, very low to low storage capacity, and a capacitive part of the system that is: (*i*) small and poorly developed; (*ii*) contributes little or nothing to runoff; or (*iii*) drains rapidly. However, the system has a relatively inertial operation, with a high regulation time for its class.

Cents-Fonts, Homede, and Boundoulaou are classified as systems with a high level of karstification, allowing rapid water transfer, low to medium storage capacity, and with a moderately developed capacitive part that drains moderately. The analysis of the regulation time suggests medium inertia for the Cents-Fonts system, and high inertia for the Homede and Boundoulaou systems.

This classification is consistent with descriptions found in the literature and studies carried out on each system (Ladouche et al., 2006; Moussu, 2011; Dubois et al., 2020).

4.6 Application of the typology to a large number of systems

Systems

In order to further check the relevance of the typology, and its capacity to differentiate karst systems, the classification methodology was tested on a dataset of 78 karst systems, with different characteristics (e.g. size of the catchment, rainfall regime, climate, and degree of karstification). Thirty-four systems are in France, and data were downloaded from a database provided by the French state (Banque Hydro). The other 44 were taken from the WoKaS database (Olarinoye et al., 2020) and are distributed throughout the world.

Results

The results of the analyses, presented in Appendix F and Figure 8, enabled systems to be ranked based on the methodology presented in Figure 7 (n = 78):

- Class 1: 19 systems
- Class 2: 31 systems
- Class 3: 7 systems
- Class 4: 11 systems
- Class 5: 9 systems

A total of 57 systems have a $k_{max} \leq 0.4$, corresponding to very low to medium storage capacity (Classes 1, 2, and 3). The other 20 have higher storage capacity (Classes 4 and 5). Class 2 is most represented, which is unsurprising given that it corresponds to the archetype of karst: a system with low to medium storage capacity, with moderate emptying of the capacitive part of the system, and a considerable degree of karstification.

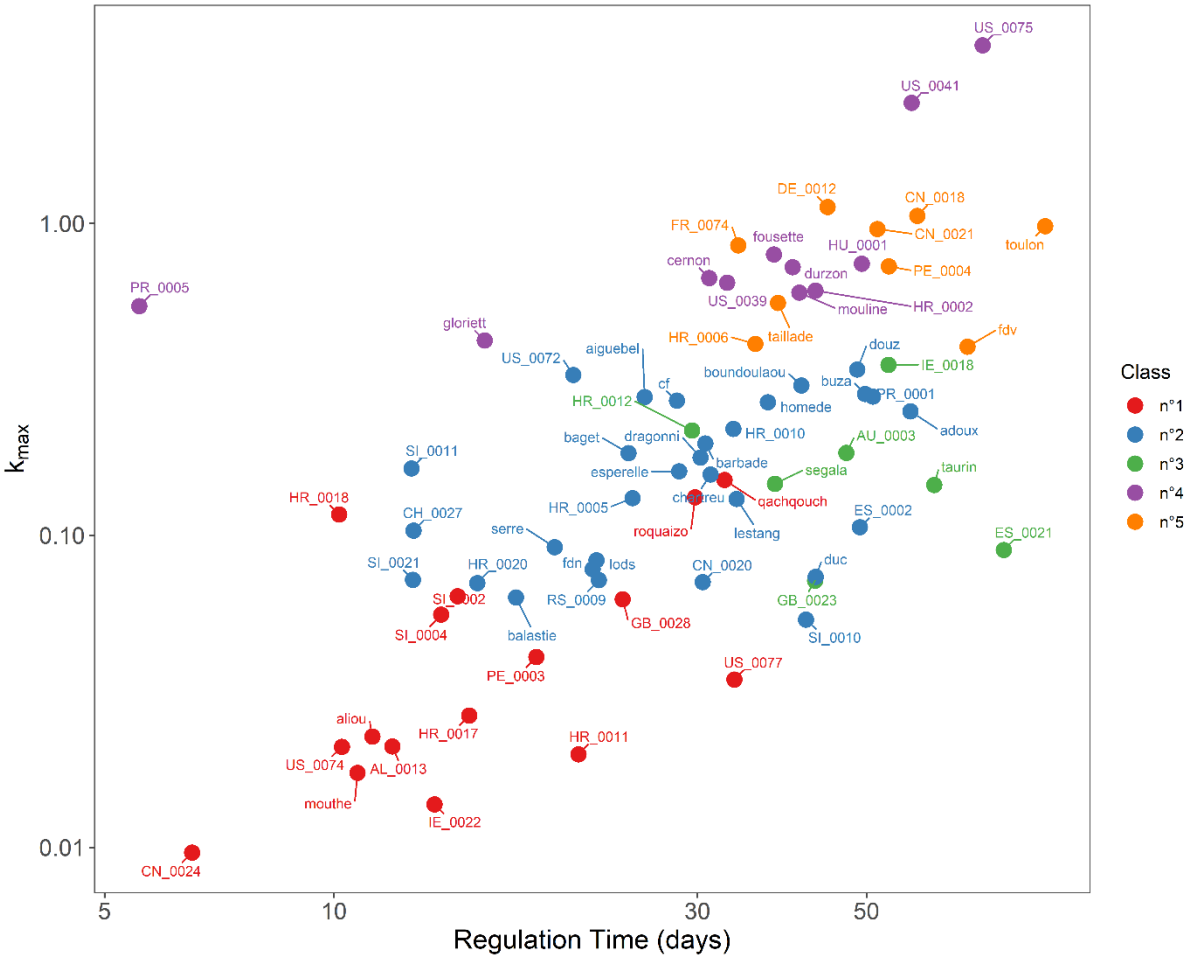

Figure 8: Graphical representation of the studied systems and their class, with k_{max} on the y-axis and regulation time on the x-axis.

Regulation time was used to differentiate between systems based on the overall inertial character of their operation. The distribution of values is consistent between classes (Figure 9). Mean regulation

time increases for Classes 1, 2, and 3, which is logical given the physical description of these systems. The same applies to Classes 4 and 5, although the differentiation is less marked.

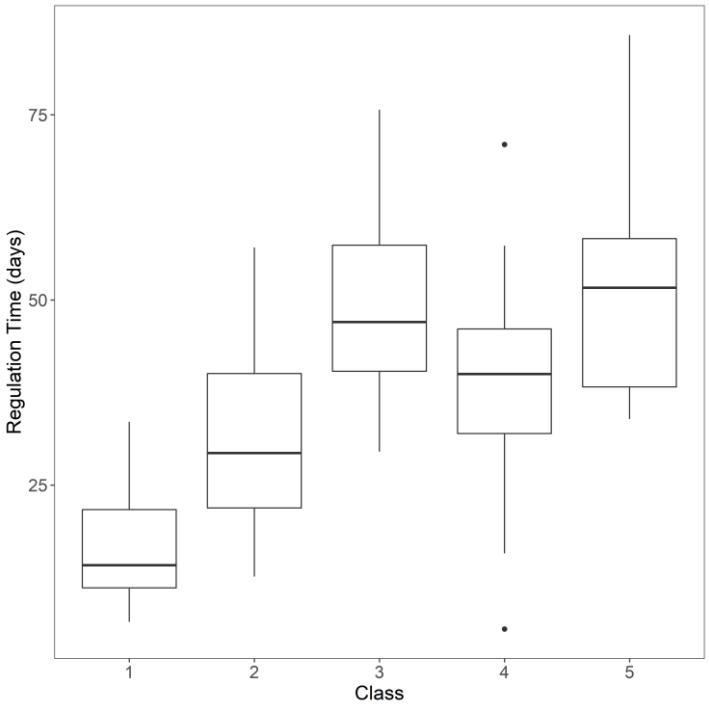

Figure 9: Boxplot of the regulation time of the studied systems within each class of the typology.

5 The future development of the typology

5.1 Using an existing model and the parameters of the equation

5.1.1 The Padilla model

The direct interpretation of α and n in the Padilla model is not particularly useful because of the problem of equifinality. However, Q_c systematically converges to a single value and can be used for interpretation. Our research led to the development of two indicators that represent influenced and non-influenced regimes. In order to evaluate their relevance, they were compared with Mangin's indicators, *i* and *k.*

Influenced regime

The influenced regime can be characterized, like Mangin's *i,* by observing the value of the model *t* days after the flood peak, expressed as a relative proportion of the flood discharge. To ensure consistency, *Qc*, which may correspond to a low discharge associated with flows in the saturated zone, was subtracted from the obtained discharge to examine the part of the discharge corresponding to the influenced regime. Appendix G shows recession curves for all studied recessions, simulated with the Padilla model by subtracting the discharge Q_c. The most relevant distribution of the model's values corresponds to the time t = 3 days; at this point, values can be distinguished, and are representative of the operation of the system.

p characterizes the capacity of the system to filter precipitation. It is calculated as:

$$p = \frac{(Q_0 - Q_c)[1 + (n-1)\alpha_0 * 3]^{\frac{n}{(1-n)}}}{Q_0} \quad (5)$$

The results are in agreement with Mangin's indicator *i* (Appendix H, graphs (B), (D) and (F)), except for the Toulon system, where values are considerably lower, and therefore inconsistent with the operation of the system.

The R^2 was 0.915 and Kendall's coefficient was 0.855, indicating good agreement between the two indicators.

Like *i*, *p* is a function of the saturation of the system, and variability in the results can measured by a new indicator, based on the standard deviation of *p*.

Non-influenced regime

Although Q_c does not necessarily have any particular physical meaning, values are consistent with the hypothesis that this discharge corresponds to discharge from areas of the system with low transmission. To a certain extent, it can be used to characterize the non-influenced regime, i.e. the storage and restitution capacity of reserves, by evaluating the ratio of Q_c to the mean interannual discharge.

qcm is calculated as follows:

$$qcm = \frac{Q_c}{Q_{mean}} \quad (6)$$

The results are approximately consistent with Mangin's *k* (Appendix H, graphs (A), (C) and (E)).

The R^2 was 0.818 and Kendall's coefficient was 0.657, indicating good agreement between the two indicators.

5.1.2 The hyperbolic model

It is possible to consider the direct interpretation of *α* and *n* in the hyperbolic model, as there are no equifinality problems. However, the analysis of the derivative and the distribution of parameters in the different systems (Appendix I) highlights some limitations:

- *α* and *n* seem to be interdependent. The consequence is that the amplitude of *α* is large, and the distribution of parameters is inconsistent (i.e. for the *fdn* system: *α* is very low and *n* is high);
- System differentiation seems to be negligible compared with the results obtained with the Mangin indicators.

The analysis of the derivative is as follows:

$$\frac{dQ}{dt} = Q_0 * -\frac{\alpha n}{1 + \alpha t} \quad (7)$$

$$\frac{dQ}{Q_0} = -\frac{\alpha n * dt}{1 + \alpha t}$$

$$25 \quad (8)$$

5.2 Improving an existing model

Section 2.2 compared and identified three models (hyperbolic, Mangin, and Padilla). All three can correctly simulate recession in karst hydrosystems. In the context of our study, the hyperbolic and Padilla models are most useful, because they do not require any action on the part of the user (unlike the Mangin model, which requires the definition of the inflection point). Our work therefore focused on the former two models.

An analysis of the performance of the hyperbolic model (Figure 2) highlights that it struggles to reproduce both influenced and non-influenced regimes. This, together with a visual analysis of poor calibrations (Appendix J), indicates the following weaknesses:

- The model fails to reflect 'intermediate' discharges, located in the hollow of the curve;
- The model produces an over-estimation of the fall in the non-influenced regime, which leads to an under-estimation of the discharge at the end of the recession limb.

These weaknesses were addressed by adding *Qc*, following the approach adopted by Padilla et al. (1994) to address the Coutagne (1949) equation:

$$Q_t = \frac{Q_0 - Q_c}{(1 + \alpha t)^n} + Q_c \tag{9}$$

where Q_0 is the discharge at time $t = 0$, α is the recession coefficient, n is a constant that is a function of the geometry of the catchment. Although Q_c has no particular physical meaning, it can, nevertheless, be assimilated to a discharge from aquitards outside the karst system, or the discharge in zones where transmission is low within the aquifer. In order to maintain a certain degree of coherence with any potential physical reality, we defined $Q_c \geq 0$.

5.2.1 Performance of the new model

Results from the proposed model (called the Qc-hyperbolic model) are very good with a relative error of 5.1% for fast flows, and 5.9% for slow flows. The mean Nash criterion was 0.984 (Figure 10). These results show that adding a new parameter to the hyperbolic equation considerably improves the model's performance. A visual analysis of recession curves confirms that the weaknesses initially identified in the hyperbolic model are corrected by the addition of Q_c (Appendix K).

Sensitivity analyses highlighted slight equifinality issues with respect to α and n, which may make direct interpretation difficult.

5.2.2 Ways forward for the typology

Use of parameters in the Qc-hyperbolic model

The model's parameters lack reliability, and are not sufficiently consistent for direct use in characterizing the operation of a system. The distribution of α and n in the new model (Appendix L) does not reveal a clear trend that would allow matching of these parameters to system characteristics.

Influenced regime

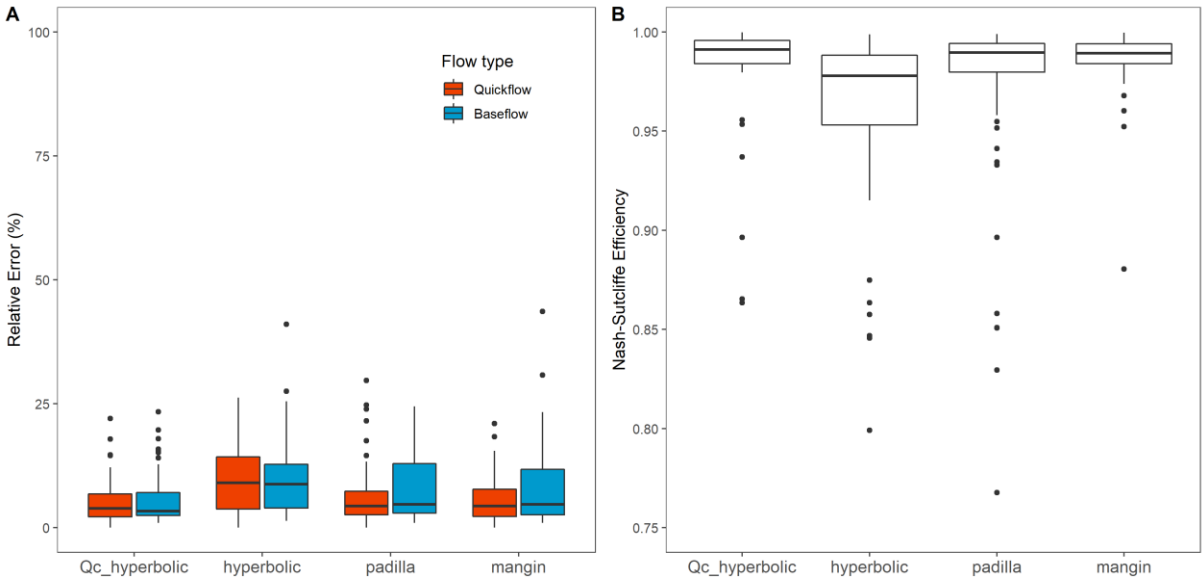

Figure 10: (A) Boxplot of errors related to the Qc-hyperbolic model compared with those in the hyperbolic, Padilla, and Mangin models for influenced and non-influenced regimes, with respect to the observed discharge over all recessions. (B) Boxplot of Nash criteria resulting from the calibration of the different models over all observed recessions.

Like *p* in the Padilla model, it is possible to define an indicator (*h* for the Qc-hyperbolic model) by taking the model value *t* days after the flood peak, expressed as a percentage of the flood discharge. Q_c, which may correspond to low discharge associated with flows in the saturated zone, is subtracted from the obtained discharge in order to characterize the part of the discharge corresponding to the influenced regime. Appendix M shows recession curves for all of the studied recessions simulated with the Qc-hyperbolic model, by subtracting the discharge Q_c. Performance is best at time t = 2 days. At this point, values can be distinguished, and are representative of the operation of the system.

h is calculated as follows:

$$h = \frac{(Q_0 - Q_c)}{(1 + \alpha * 2)^n} \frac{1}{Q0} \quad (10)$$

The results obtained are consistent with how systems are known to function, and very similar to those obtained for the Mangin model (Appendix N). The correlation between *h* and *i* is excellent, with R^2 of 0.908 and a Kendall coefficient of 0.863.

Like *i*, *h is* a function of the saturation of the system, and variability in results can be modeled by a new indicator, based on the standard deviation of *h.*

Non-influenced regime

Characterization of the functioning of the saturated zone with the Qc-hyperbolic model proved to be difficult. In some cases, *Qc* is null, making the indicator unusable. Several ways forward are being studied with the objective of being able to analyze the non-influenced regime and characterize the storage and restitution of precipitation.

5.3 Approximation of indicators found in the literature

We also sought to assess whether the indicators proposed by Mangin (1975) could be approximated by simple indicators. The idea was to simplify an existing approach by removing the need to calibrate recession models, while maintaining consistent results.

Influenced regime. Mangin's *i* characterizes the capacity of a system to filter rainfall. Like *p* and *h*, it can be approximated by dividing the discharge at time t = 2 days by the initial peak flood discharge. This approach is similar to the calculation of *i,* with the difference that the entire discharge is considered, unlike the calculation of *i*, which is only based on the part of the discharge corresponding to the influenced regime.

The results are very interesting (Appendix O, graphs (B), (D), and (F)). The R^2 was 0.912 and the Kendall coefficient was 0.806.

Like *i,* variability in the results can be modeled by a new indicator based on the standard deviation of the initial indicator.

Non-influenced regime. Mangin's *k* (1975) characterizes the capacity of a system to store and restitute precipitation. It corresponds to the ratio of the dynamic volume to the mean interannual volume, the dynamic volume being calculated from the drying coefficient α from the exponential model. In some ways, this coefficient, which characterizes the emptying of a reservoir with low transmissivity, is a function of the length of the recession under consideration, and the discharge at the end of the drying period.

The ratio of the end-of-drying discharge to the mean interannual discharge is similar to Mangin's *k* (Appendix O, graphs (A), (C) and (E)). The R^2 was 0.887 and the Kendall coefficient was 0.738, indicating good agreement between the two indicators.

5.4 Analysis of electrical conductivity series at the outlet of systems

The analysis of electrical conductivity series may supplement information derived from analyses of flow time series. Although, like discharge, conductivity can be measured with autonomous probes at high frequency, there are far fewer instrumented systems, making it difficult to base a typology on the analysis of electrical conductivity. Nevertheless, as series were available for nine of the ten systems in our dataset, this analysis was able to be conducted.

5.4.1 State-of-the-art

Electrical conductivity is the ability of a solution to conduct an electric current (Hubert and Wolkersdorfer, 2015). It is a function of the concentration of gases and dissolved elements (Pelkie et al., 1992), along with colloids and suspended solids (McNeil and Cox, 2000) and is affected by temperature, pressure, discharge, and any dissolved elements (McNeil and Cox, 2000). It is expressed as *µS/cm* or *mS/cm*, and is influenced by the following parameters:

- **temperature,** which affects the mobility of ions in solution. Conductivity measurements are only comparable if they are converted to the same reference temperature (Hubert and Wolkersdorfer, 2015), usually 25°C;
- **the valence and mobility of each ionic species** (McNeil and Cox, 2000), i.e. their specific electrical conductivity. A change in the distribution of dissolved species (facies) can change

electrical conductivity without necessarily modifying the total concentration, by changing ion ratios (Marandi et al., 2013).

Table 10: Conductivity indicators for the studied systems.

System	Average conductivity *µS/cm*	Coefficient of variation %	Minimum conductivity *µS/cm*	Maximum conductivity *µS/cm*	Amplitude *µS/cm*
Baget	326.5	3.4	243	372	129
Durzon	429.5	4.7	376	486	110
Esperelle	452.4	2.7	399	487	88
Fdn	918.7	28.5	479	2528	2049
Fdv	447.7	5.5	360	496	136
Lods	538.9	5.3	431	643	212
Mouline	408.1	4.8	317	477	160
Mouthe	335.9	8.8	206	415	209
Toulon	580.5	2.2	518	601	83

The range of variation in electrical conductivity differs as a function of the hydrosystem under consideration. It is mainly a function of the size of the catchment and the degree of karstification. These factors partly shape the length of time water remains and, therefore, its degree of mineralization.

5.4.2 Analysis of the dataset

Table 10 and Appendix P present the results of our statistical analyses.

Conclusion

The various methods used to analyze discharge time series at the outlet of karst systems can characterize several aspects of their operation. The analysis of recession curves is a particularly appropriate way to distinguish influenced and non-influenced flow regimes of spring discharge, and many authors have proposed typologies based on this method.

The first aim of our study was to identify ways to update existing typologies:

- Our examination of different recession models identified that several would be useful in the development of a typology. One way forward is to integrate variability in the hydrodynamic functioning of a system in order to differentiate stable, regular systems from systems in which saturation or the distribution of precipitation impacts hydrodynamic functioning;
- The inclusion of indicators from correlational and spectral analyses can refine the classification obtained from the analysis of recession curves, and characterize overall system inertia;
- The classified spring discharge analysis helps to identify specific system functions, such as the activation of overflow outlets and a change in flow properties. We propose a generic method, which aims to simplify the analysis and identify the presence or absence of major specific behaviors and system characteristics.

In a second step, we tested our proposed typology on a large dataset made up of systems distributed around the world. Here, the objective was to observe the distribution of systems within classes, and to study the influence of climate. Our results show that the typology is robust, and can clearly differentiate between systems.

Our proposed typology appears to be a relevant way to characterize karst systems, based on the study of flow time series. We are already looking at numerous options for further work:

- The development of a recession model that does not require operator intervention. The objective is twofold: to reduce bias, and to reduce the execution time for the analysis;
- The inclusion of hydrochemical aspects, through the analysis of conductivity and temperature series. In general, although fewer series are available, conductivity can be monitored at high frequency;
- The examination of climate and mean precipitation based on the study of climate at different scales (from the Köppen–Geiger classification to the analysis of rainfall measures).

Finally, the medium-term objective is to link the classification of karst systems and modeling their functioning. This would help in the design of models, and limit the choice of parameters.

References

Alfaro, C. and Wallace, M. (1994). Origin and classification of springs and historical review with current applications. *Environmental Geology*, 24(2):112–124.

Barnes, B. S. (1939). The structure of discharge-recession curves. *Transactions, American Geophysical Union*, 20(4):721.

Berry, M. and Linoff, G. (1996). *Data Mining Techniques for Marketing, Sales, and Customer Support*. USA, john wiley & sons, inc. edition.

Blavoux, B., Mudry, J., and Puig, J.-M. (1992). Bilan, fonctionnement et protection du système karstique de la Fontaine de Vaucluse (sud-est de la France). *Geodinamica Acta,* 5(3):153–172.

Boussinesq, J. (1878). *Essai Sur La Théorie Des Eaux Courantes*. PhD thesis.

Box, G. and Jenkins, G. (1976). *Time Series Analysis : Forecasting and Control*. San Francisco, holden day edition.

Brillinger, D. (1975). *Time Series Data Analysis and Theory*. New York, holt, rinehart & winston edition.

Cinkus, G. (2020). Caractérisation de la réponse hydrodynamique d'aquifères karstiques. Proposition d'une typologie. Master's thesis, 51 p, HydroSciences Montpellier.

Coutagne, A. (1949). ÉTUDE GÉNÉRALE DES VARIATIONS DE DÉBIT EN FONCTION DES FACTEURS QUI LES CONDITIONNENT. *La Houille Blanche,* (2):134–146.

Dörfliger, N. (2010). Guide méthodologique, Les outils de l'hydrogéologie karstique. Avec la collaboration de Ph. Crochet, R. Guerin, N. Jozja, B. Marsaud, P-H. Mondain, Ph. Muet, V. Plagnes. *BRGM RP58237-FR*, page 246.

Drogue, C. (1972). Analyse statistique des hydrogrammes de decrues des sources karstiques statistical analysis of hydrographs of karstic springs. *Journal of Hydrology,* 15(1):49–68.

Dubois, E., Doummar, J., Pistre, S., and Larocque, M. (2020). Calibration of a semi-distributed lumped karst system model and analysis of its sensitivity to climate conditions: The example of the Qachqouch karst spring (Lebanon). Preprint, Groundwater hydrology/Modelling approaches.

Flora, S. P. (2004). *Hydrogeological Characterization and Discharge Variability of Springs in the Middle Verde River Watershed, Central Arizona*. PhD thesis, Northern Arizona University.

Forkasiewicz, M. J. and Paloc, H. (1967). Régime de tarissement de la foux-de-la-vis (Gard) étude préliminaire. *La Houille Blanche*, (1):29–36.

Gan, G., Ma, C., and Wu, J. (2007). *Data Clustering: Theory, Algorithms, and Applications.* Asasiam series on statistics and applied probability edition.

Govender, P. and Sivakumar, V. (2020). Application of k-means and hierarchical clustering techniques for analysis of air pollution: A review (1980–2019). *Atmospheric Pollution Research,* 11(1):40–56.

Gower, J. C. and Legendre, P. (1986). Metric and Euclidean properties of dissimilarity coefficients.

Journal of Classification, 3(1):5–48.

Grasso, D. and Jeannin, P.-Y. (1994). étude critique des méthodes d'analyse de la réponse globale des systèmes karstiques. Application au site de Bure (JU, Suisse). *Bulletin d'Hydrogéologie,* (13):26. Halkidi, M. (2001). On Clustering Validation Techniques. page 39.

Hannan, E. (1970). *Multiple Time Series.* New York, wiley edition.

Horton, R. E. (1933). The Rôle of infiltration in the hydrologic cycle. *Transactions, American Geophysical Union*, 14(1):446.

Hubert, E. and Wolkersdorfer, C. (2015). Establishing a conversion factor between electrical conductivity and total dissolved solids in South African mine waters. *Water SA,* 41(4):490.

Jain, A. K., Murty, M. N., and Flynn, P. J. (1999). Data clustering: A review. *ACM Computing Surveys (CSUR)*, 31(3):264–323.

Jeannin, P.-Y. and Sauter, M. (1998). Analysis of karst hydrodynamic behaviour using global approaches: A review. (16):18.

Jenkins, G. and Watts, D. (1968). *Spectral Analysis and Its Applications.* San Francisco, holden day edition.

Jourde, H.,Massei N., Mazzilli N., …, and Wang X. (2018) SNO KARST: A French Network of Observatories for the Multidisciplinary Study of Critical Zone Processes in Karst Watersheds and Aquifers. Vadose Zone J. 17:180094.http://dx.doi.org/10.2136/vzj2018.04.0094Kovács, A. (2003). *Geometry and Hydraulic Parameters of Karst Aquifers: A Hydrodynamic Modeling Approach*. PhD thesis, Neuchâtel.

Kresic, N. (2007). *Hydrogeology and Groundwater Modeling, 2nd Edn*.

Kullman, E. (2000). Nové metodické prístupy k riešeniu ochrany a ochranných pásiem zdrojov podzemných vôd v horninových prostrediach s krasovo – puklinovou priepustnosťou. *Podzemná voda,* VI.:31–41.

Ladouche, B., Maréchal, J.-C., Dörfliger, N., and Lachassagne, P. (2006). Étude réalisée dans le cadre du projet de recherche EAUR15 COMPLEX'AQUI du BRGM. page 277.

Larocque, M., Mangin, A., Razack, M., and Banton, O. (1998). Contribution of correlation and spectral analyses to the regional study of a large karst aquifer (Charente, France). *Journal of Hydrology,* 205(3-4):217–231.

Lorette, G., Lastennet, R., Peyraube, N., and Denis, A. (2018). Groundwater-flow characterization in a multilayered karst aquifer on the edge of a sedimentary basin in western France. *Journal of Hydrology,* 566:137–149.

Maillet, E. T. (1905). *Essais d'hydraulique Souterraine et Fluviale*. Mécanique et Physique Du Globe. Paris, a. hermann edition.

Malik, P. (2006). Assessment of regional karstification degree and groundwater sensitivity to pollution using hydrograph analysis in the Velka Fatra Mountains, Slovakia. *Environmental Geology,* 51(5):707–711.

Malík, P. (2015). Evaluating Discharge Regimes of Karst Aquifer. In Stevanović, Z., editor, *Karst Aquifers—Characterization and Engineering*, pages 205–249. Springer International Publishing, Cham.

Malík, P. and Vojtková, S. (2012). Use of recession-curve analysis for estimation of karstification degree and its application in assessing overflow/underflow conditions in closely spaced karstic springs. *Environmental Earth Sciences*, 65(8):2245–2257.

Mangin, A. (1970). Contribution à l'étude d'aquifères karstiques à partir de l'analyse de courbes de décrues et de tarissements. *Annales de Spéléologie*, 25(3):581–609.

Mangin, A. (1971). étude des débits classés d'exutoires karstiques portant sur un cycle hydrologique. *Annales de Spéléologie*, 26(2):283–329.

Mangin, A. (1975). Contribution à l'étude hydrodynamique des aquifères karstiques. page 268.

Mangin, A. (1984). Pour une meilleure connaissance des systèmes hydrologiques à partir des analyses corrélatoire et spectrale. page 19.

Marandi, A., Polikarpus, M., and Jõeleht, A. (2013). A new approach for describing the relationship between electrical conductivity and major anion concentration in natural waters. *Applied Geochemistry*, 38:103–109.

Marsaud, B. (1997). *Structure et Fonctionnement de La Zone Noyée Des Karsts à Partir Des Résultats Expérimentaux.* PhD thesis.

Massei, N., Dupont, J., Mahler, B., Laignel, B., Fournier, M., Valdes, D., and Ogier, S. (2006). Investigating transport properties and turbidity dynamics of a karst aquifer using correlation, spectral, and wavelet analyses. *Journal of Hydrology*, 329(1-2):244–257.

McNeil, V. H. and Cox, M. E. (2000). Relationship between conductivity and analysed composition in a large set of natural surface-water samples, Queensland, Australia. *Environmental Geology,* 39(12):1325–1333.

Meinzer, O. (1923). *Outline of Ground-Water Hydrology*. Usgs water-supply paper edition.

Milligan, G. W. and Cooper, M. C. (1987). Methodology Review: Clustering Methods. *Applied Psychological Measurement*, 11(4):329–354.

Moussu, F. (2011). *Prise En Compte Du Fonctionnement Hydrodynamique Dans La Modélisation Pluie Débit Des Systèmes Karstiques*. PhD thesis, Pierre et Marie Curie, Paris VI.

M. Mudarra, B. Andreo (2011). Relative importance of the saturated and the unsaturated zones in the hydrogeological functioning of karst aquifers: The case of Alta Cadena (Southern Spain). *Journal of Hydrology*, 397(3–4) :263-280. ISSN 0022-1694, https://doi.org/10.1016/j.jhydrol.2010.12.005.

Netopil, R. (1971). The classification of water springs on the basis of the variability of yields. *Studia Geographica*, (22):145–150.

Olarinoye, T., Gleeson, T., Marx, V., Seeger, S., Adinehvand, R., Allocca, V., Andreo, B., Apaéstegui, J., Apolit, C., Arfib, B., Auler, A., Barberá, J. A., Batiot-Guilhe, C., Bechtel, T., Binet, S., Bittner, D., Blatnik, M., Bolger, T., Brunet, P., Charlier, J.-B., Chen, Z., Chiogna, G., Coxon, G., De Vita, P., Doummar, J., Epting, J., Fournier, M., Goldscheider, N., Gunn, J., Guo, F., Guyot, J. L., Howden, N., Huggenberger, P., Hunt, B., Jeannin, P.-Y., Jiang, G., Jones, G., Jourde, H., Karmann, I., Koit, O., Kordilla, J., Labat, D., Ladouche, B., Liso, I. S., Liu, Z., Massei, N., Mazzilli, N., Mudarra, M., Parise, M., Pu, J., Ravbar, N., Sanchez, L. H., Santo, A., Sauter, M., Sivelle, V., Skoglund, R. Ø., Stevanovic, Z., Wood, C., Worthington, S., and Hartmann, A. (2020). Global karst springs hydrograph dataset for research and management of the world's fastest-flowing groundwater. *Scientific Data,* 7(1):59.

Padilla, A. and Pulido-Bosch, A. (1995). Study of hydrographs of karstic aquifers by means of correlation and cross-spectral analysis. *Journal of Hydrology*, page 17.

Padilla, A., Pulido-Bosch, A., and Mangin, A. (1994). Relative Importance of Baseflow and Quickflow from Hydrographs of Karst Spring. *Ground Water*, 32(2):267–277.

Pelkie, J. E., Concannon, P. J., Manley, D. B., and Poling, B. E. (1992). Product distributions in the carbon dioxide-ammonia-water system from liquid conductivity measurements. *Industrial & Engineering Chemistry Research*, 31(9):2209–2215.

Shirkhorshidi, A. S., Aghabozorgi, S., and Wah, T. Y. (2015). A Comparison Study on Similarity and Dissimilarity Measures in Clustering Continuous Data. *PLOS ONE*, 10(12):e0144059.

Springer, A. E., Stevens, L. E., Anderson, D. E., Parnell, R. A., Kreamer, D. K., Levin, L., and Flora, S. P. (2004). CHAPTER 4 A COMPREHENSIVE SPRINGS CLASSIFICATION SYSTEM: INTEGRATING GEOMORPHIC, HYDROGEOCHEMICAL, AND ECOLOGICAL CRITERIA. page 31.

Thiéry, D. (2018). Modélisation hydrologique globale des débits de 23 sources karstiques avec le logiciel ÉROS. *Rapport BRGM/RP-67723-FR*, page 66.

Toebes, C. and Strang, D. D. (1964). ON RECESSION CURVES: 1 — Recession Equations. *Journal of Hydrology (New Zealand)*, 3(2):2–14.

Tufféry, S. (2011). *Data Mining and Statistics for Decision Making: Tufféry/Data Mining and Statistics for Decision Making*. John Wiley & Sons, Ltd, Chichester, UK.

Appendices

A Summary of the main models used to analyze recession curves. '✓' indicates that the model was selected and 'X' indicates that the model was not selected.

Model	Equation	Selection	Comment
Boussinesq (1903)	$Q_t = \frac{Q_0}{(1+\alpha t)^2}$	X	- non-influenced stage - Surface water
Maillet (1905)	$Q_t = Q_0 e^{-\alpha t}$	X	- non-influenced stage - Surface water
Horton (1933)	$Q_t = Q_0 e^{-\alpha t^n}$	X	- More suitable to surface water
Barnes (1939)	$Q_t = \sum_{i=1}^{n} Q_0 e^{-\alpha_i t}$	X	- More suitable to surface water - Hard to automate
Coutagne (1948)	$Q_t = Q_0[1+(n-1)\alpha_0 t]^{\frac{n}{(1-n)}}$	✓	+ Karst systems
Padilla et al. (1994)	$Q_t = (Q_0 - Q_c)[1+(n-1)\alpha_0 t]^{\frac{n}{(1-n)}} + Q_c$	✓	+ Karst systems + Q_c strengthens Coutagne model
Drogue (1972)	$Q_t = \frac{Q_0}{(1+\alpha t)^n}$	✓	+ Karst systems
Mangin (1975)	$Q_t = Q_{R0}{}^{e^{-\alpha t}} + q_0 \frac{1-\eta t}{1+\varepsilon t}$	✓	+ Karst systems + Exisiting typology - Bias linked to user assessment
Kullman (1990)	$Q_t = \sum_{i=1}^{n} Q_{0i} e^{-\alpha_i t} + \sum_{j=1}^{n} \left(\frac{1}{2} + \frac{\lvert 1-\beta_j t\rvert}{2(1-\beta_j t)}\right) Q_{0j}(1-\beta_j t)$	X	+ Karst systems + Exisiting typology - Hard to automate

B Selected recession curves for each dataset.

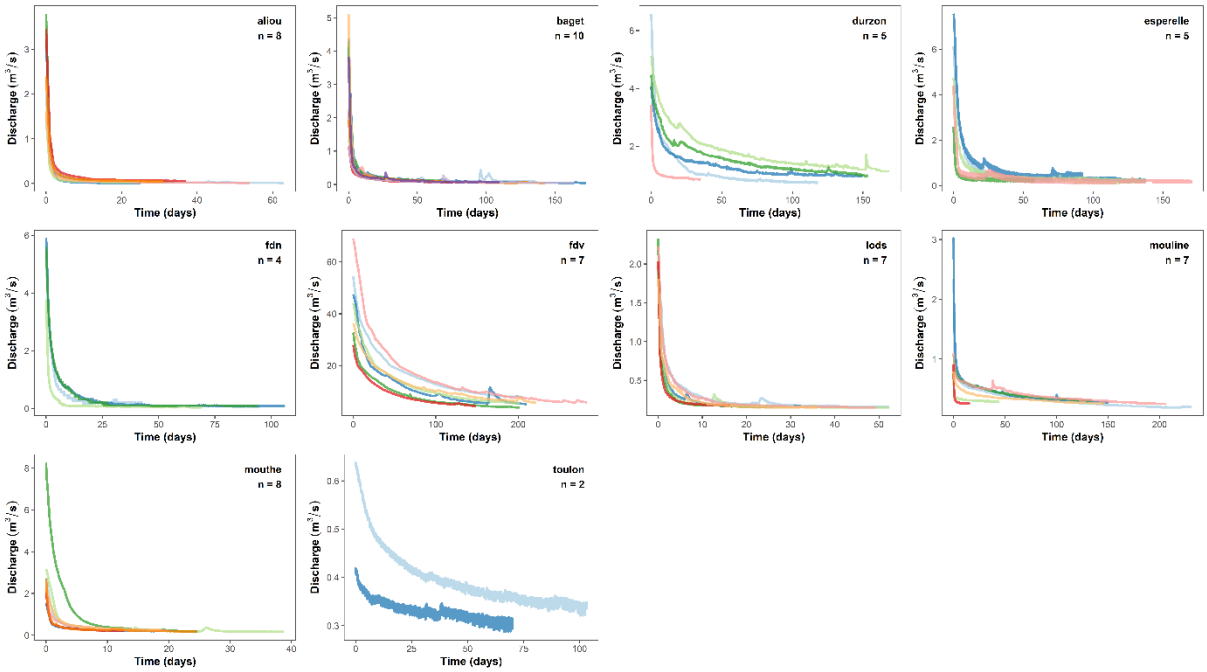

C Example of the results of the overall sensitivity analysis for four recession models for a recession in the Baget system (for the period 1977-08-29 to 1977-11-13).

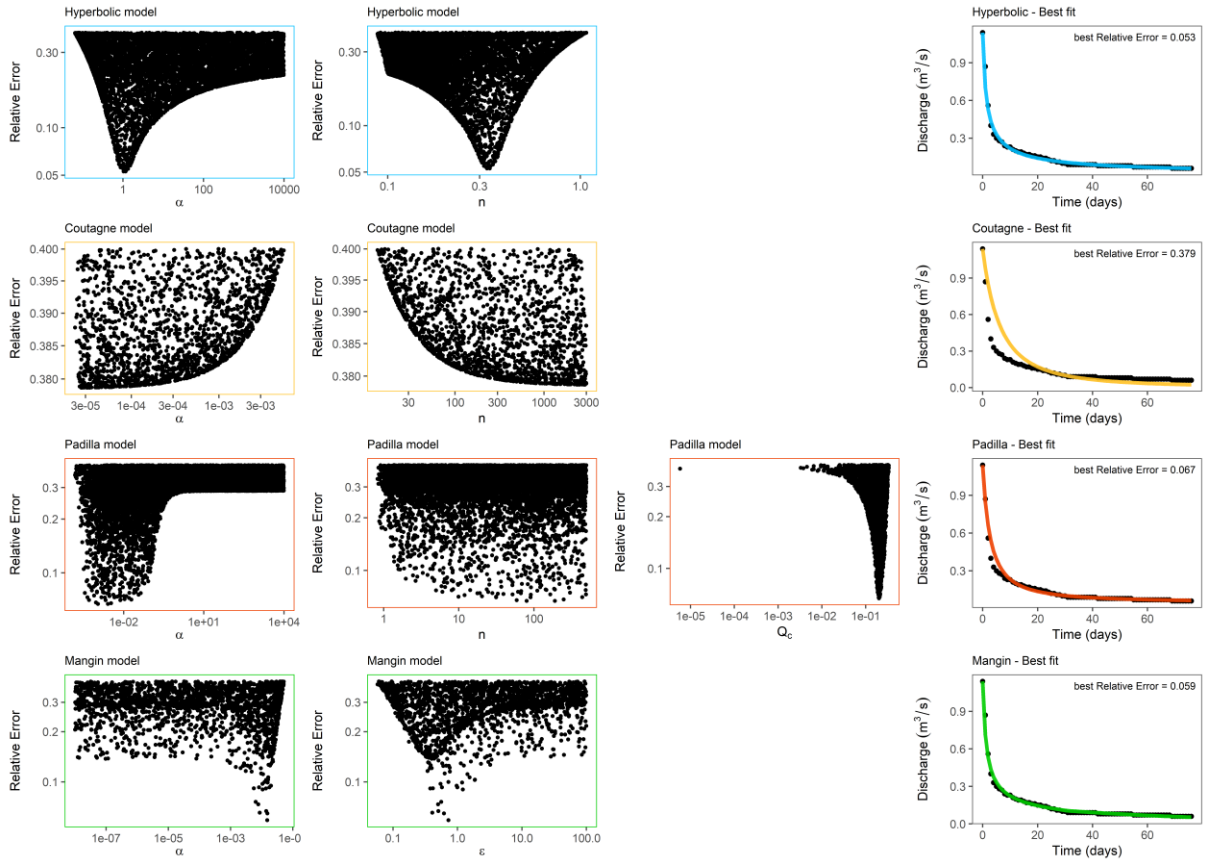

D Variability in *i* for the studied systems. The ratio of discharge in the month preceding the flood to the mean interannual discharge (Q1M) was centered-reduced to allow comparison among systems.

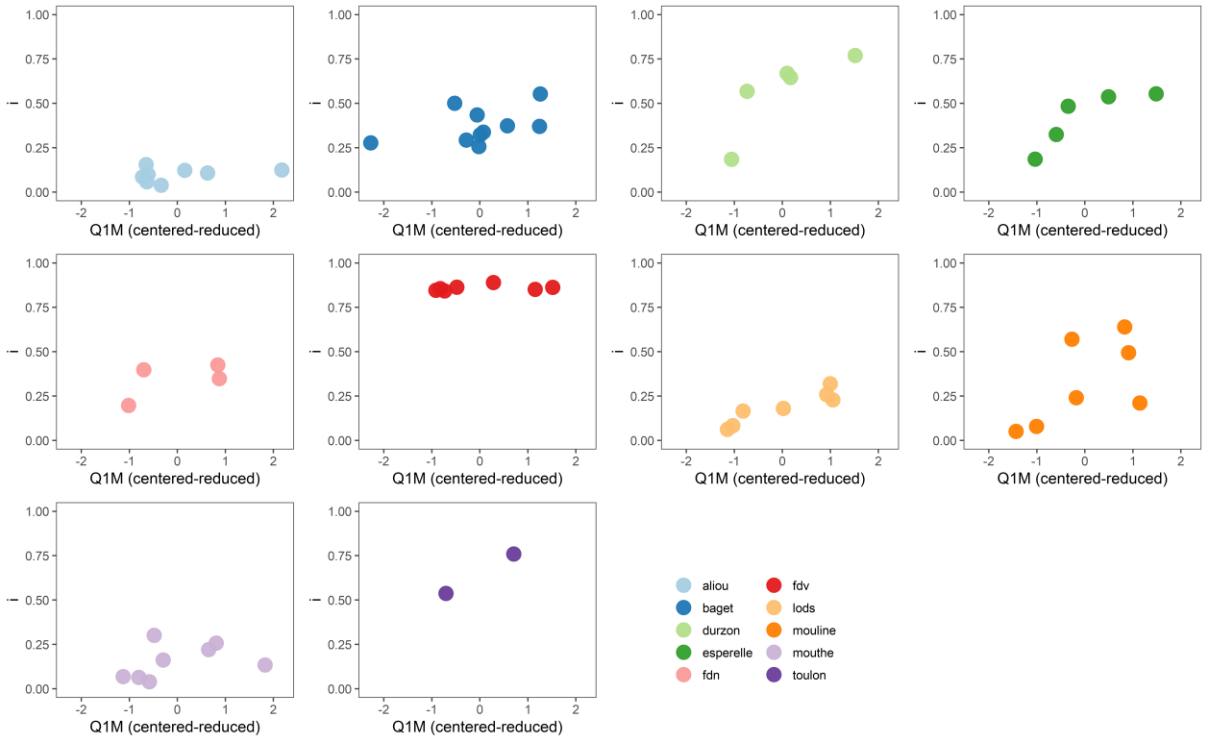

E Analysis of classified discharges for the studied systems showing the interpretation of the curve as a function of the proposed methodology.

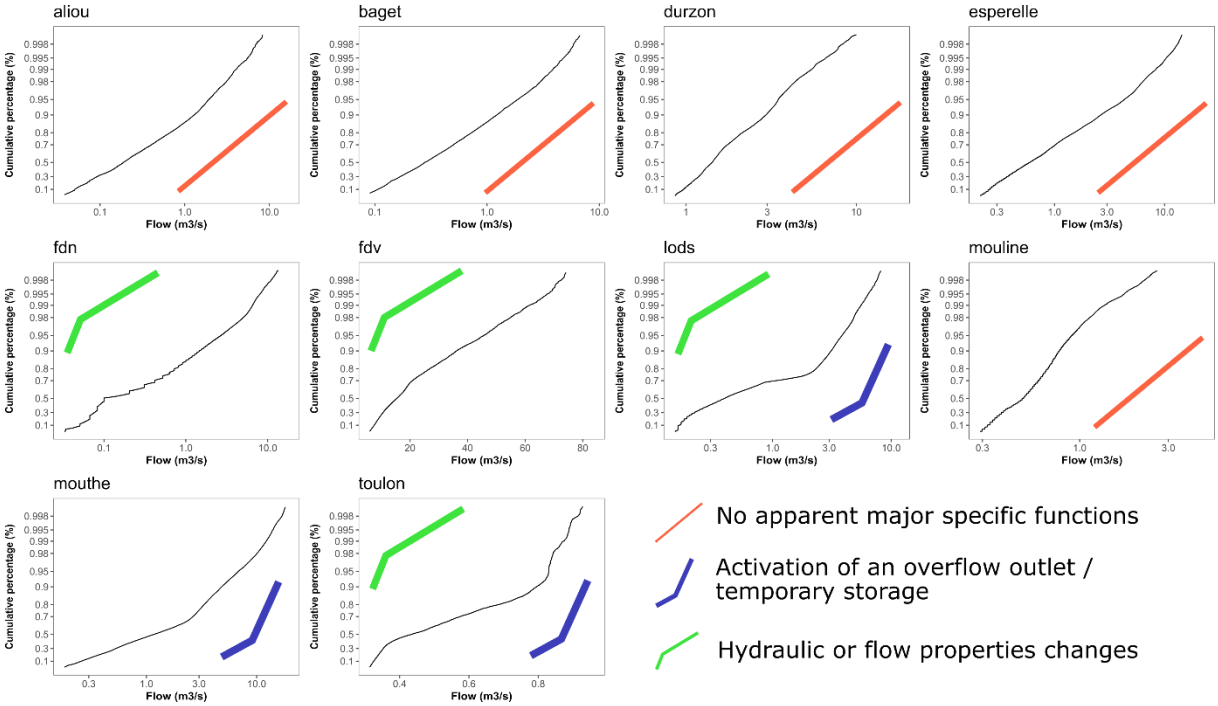

F Indicators for the dataset of 78 karst systems, sorted by class and regulation time.

System	k_{max}	i_{min}	α_{mean}	Regulation time	Class	System	k_{max}	i_{min}	α_{mean}	Regulation time	Class
CN_0024	0.01	0.02	0.187	6.5	1	**SI_0011**	0.16	0.12	0.024	12.6	2
HR_0018	0.12	0.03	0.057	10.2	1	**SI_0021**	0.07	0.10	0.022	12.7	2
US_0074	0.02	0.34	0.055	10.2	1	**CH_0027**	0.10	0.13	0.021	12.7	2
mouthe	0.02	0.04	0.041	10.7	1	**HR_0020**	0.07	0.10	0.021	15.4	2
aliou	0.02	0.04	0.063	11.2	1	**balastie**	0.06	0.27	0.023	17.3	2
AL_0013	0.02	0.09	0.095	11.9	1	**serre**	0.09	0.23	0.017	19.5	2
IE_0022	0.01	0.07	0.074	13.5	1	**US_0072**	0.33	0.05	0.013	20.6	2
SI_0004	0.06	0.15	0.045	13.8	1	**fdn**	0.08	0.20	0.012	21.8	2
SI_0002	0.06	0.17	0.047	14.5	1	**lods**	0.08	0.06	0.012	22.1	2
HR_0017	0.03	0.07	0.050	15.1	1	**RS_0009**	0.07	0.23	0.023	22.3	2
PE_0003	0.04	0.05	0.067	18.4	1	**baget**	0.18	0.26	0.014	24.4	2
HR_0011	0.02	0.00	0.161	20.9	1	**HR_0005**	0.13	0.14	0.019	24.7	2
GB_0028	0.06	0.00	0.086	23.9	1	**aiguebel**	0.28	0.34	0.009	25.6	2
roquaizo	0.13	0.19	0.034	29.8	1	**cf**	0.27	0.23	0.007	28.2	2
qachqouch	0.15	0.08	0.034	32.5	1	**esperelle**	0.16	0.19	0.011	28.4	2
US_0077	0.03	0.13	0.089	33.5	1	**dragonni**	0.18	0.34	0.014	30.3	2
stpierre	0.03	0.12	0.031	/	1	**CN_0020**	0.07	0.27	0.022	30.5	2
lez	0.17	0.44	0.076	/	1	**barbade**	0.20	0.34	0.024	30.7	2
CN_0019	0.03	0.06	0.081	/	1	**chartreu**	0.16	0.20	0.013	31.2	2
FR_0057	0.07	0.07	0.087	/	1	**HR_0010**	0.22	0.33	0.007	33.4	2
PR_0005	0.54	0.07	0.007	5.6	4	**lestang**	0.13	0.33	0.013	33.8	2
gloriett	0.42	0.16	0.006	15.8	4	**homede**	0.27	0.23	0.009	37.1	2
cernon	0.67	0.20	0.005	31.1	4	**boundoulaou**	0.30	0.33	0.009	41.0	2
US_0039	0.64	0.24	0.006	32.8	4	**SI_0010**	0.05	0.11	0.019	41.6	2
fousette	0.79	0.11	0.006	37.8	4	**duc**	0.07	0.10	0.021	42.9	2
durzon	0.72	0.19	0.004	40.0	4	**douz**	0.34	0.28	0.011	48.6	2
mouline	0.60	0.05	0.004	40.8	4	**ES_0002**	0.11	0.37	0.020	49.0	2
HR_0002	0.61	0.05	0.006	42.8	4	**buza**	0.28	0.22	0.014	49.8	2
HU_0001	0.74	0.19	0.004	49.3	4	**PR_0001**	0.28	0.00	0.008	51.0	2
US_0041	2.43	0.31	0.001	57.3	4	**adoux**	0.25	0.12	0.012	57.1	2
US_0075	3.72	0.21	0.001	71.0	4	**PE_0005**	0.15	0.20	0.027	/	2
FR_0074	0.85	0.61	0.003	33.9	5	**HR_0012**	0.22	0.68	0.010	29.5	3
HR_0006	0.41	0.58	0.005	35.7	5	**segala**	0.15	0.50	0.014	37.9	3
taillade	0.56	0.54	0.006	38.3	5	**GB_0023**	0.07	0.57	0.018	42.8	3
DE_0012	1.13	0.74	0.002	44.4	5	**AU_0003**	0.18	0.45	0.007	47.0	3
CN_0021	0.96	0.86	0.002	51.7	5	**IE_0018**	0.35	0.64	0.009	53.4	3
PE_0004	0.73	0.97	0.004	53.5	5	**taurin**	0.14	0.57	0.010	61.4	3
CN_0018	1.06	0.53	0.002	58.3	5	**ES_0021**	0.09	0.67	0.016	75.7	3
fdv	0.40	0.84	0.005	67.8	5						
toulon	0.98	0.54	0.002	85.8	5						

G All studied recessions simulated with the Padilla model. For each recession, the discharge was divided by the initial discharge to allow comparison among systems.

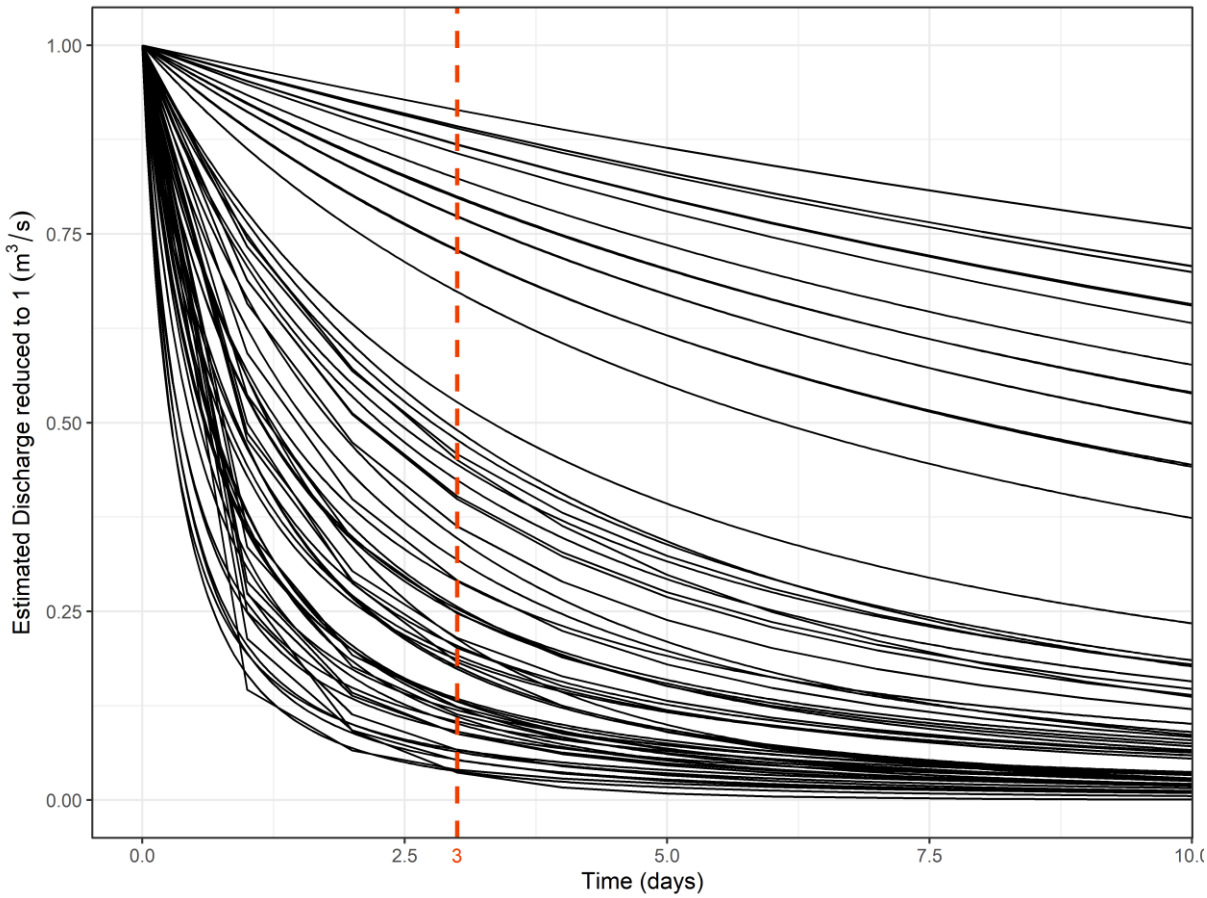

H Boxplot showing the results of indicators (A) *k* and (C) *qcm*, and (B) *i* and (D) *p*. (E) and (F) show the correlation between indicators from the Padilla model and Mangin indicators.

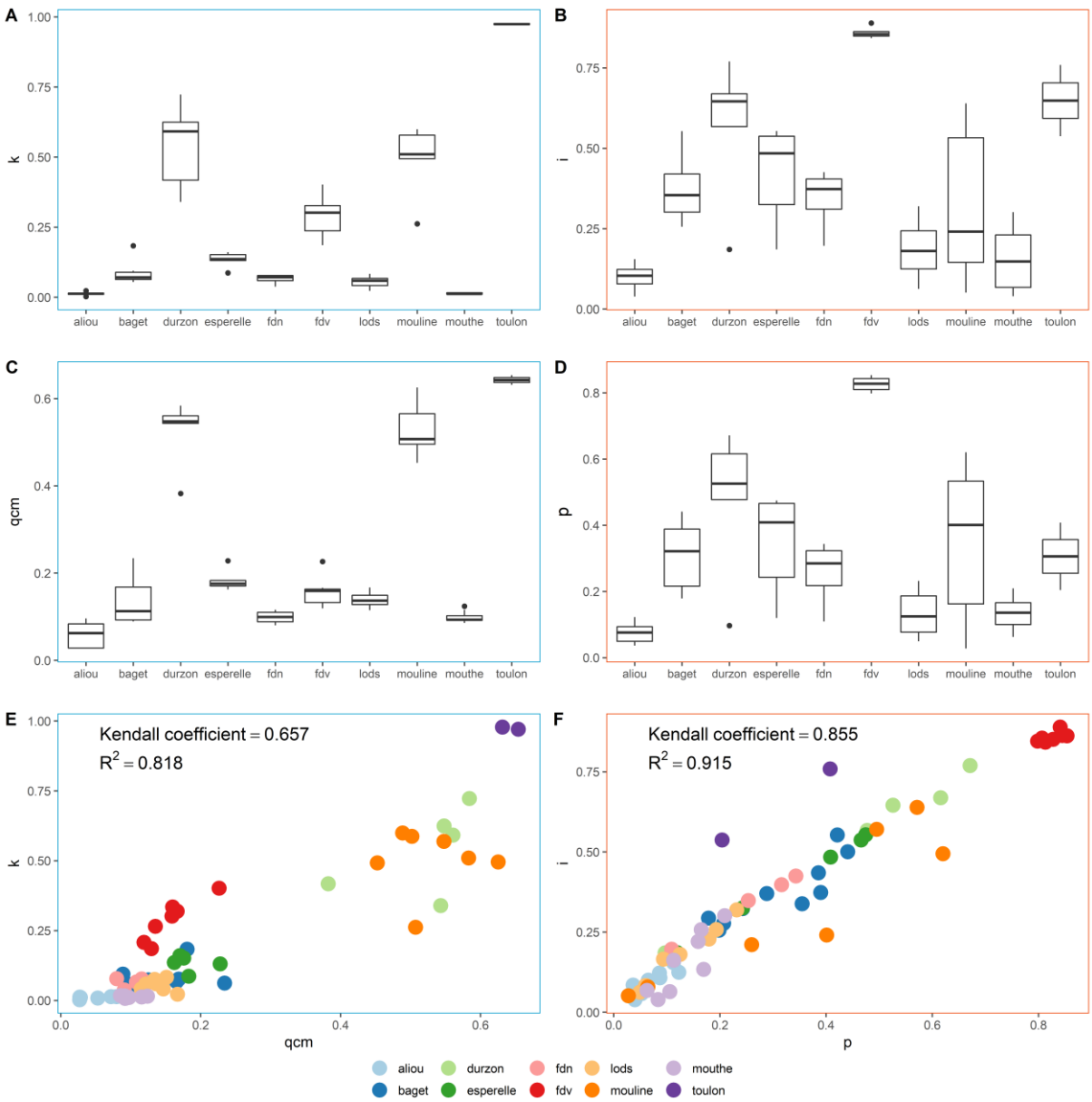

I Distribution of *α* and *n* in the hyperbolic model for the studied systems.

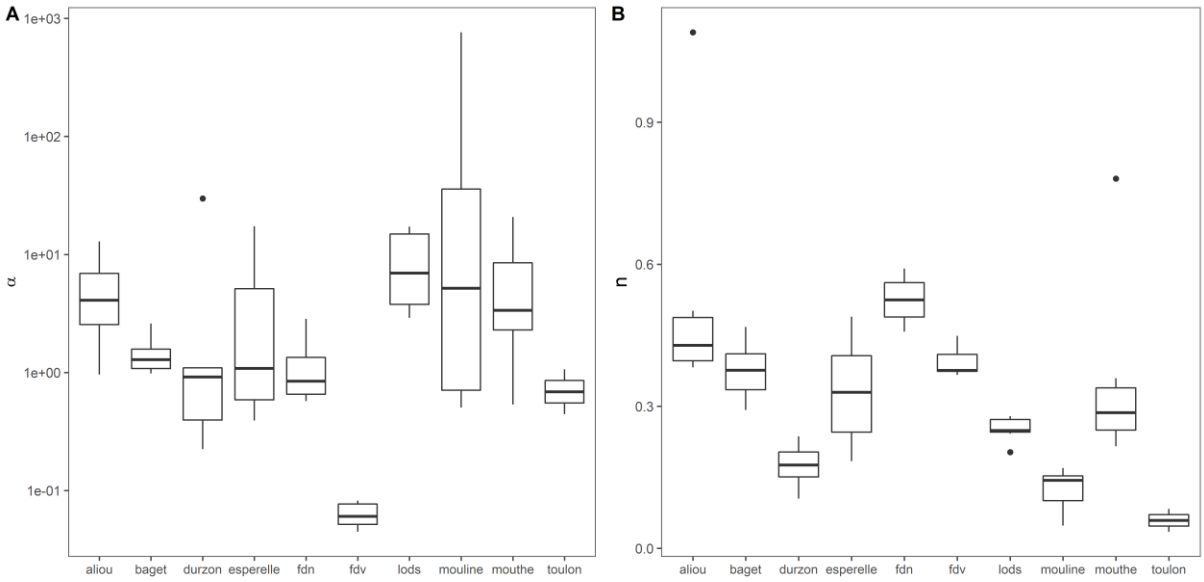

J Example of the weaknesses of the hyperbolic model for (A) Lods and (B) Mouline recessions.

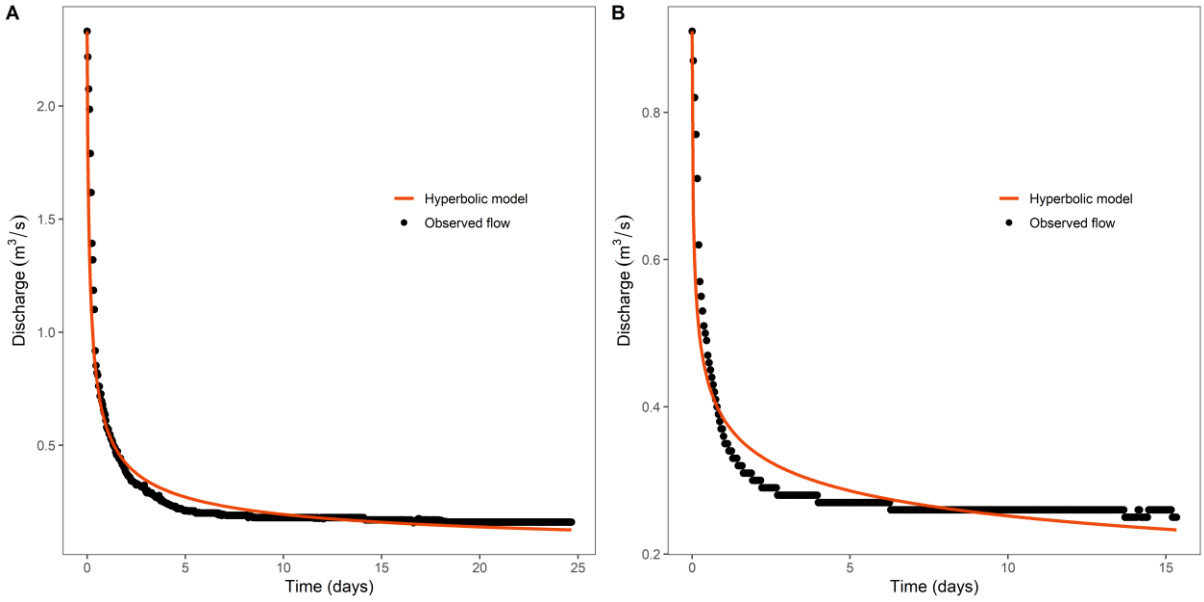

K Example of the calibration of the Qc-hyperbolic model for (A) Lods and (B) Mouline recessions.

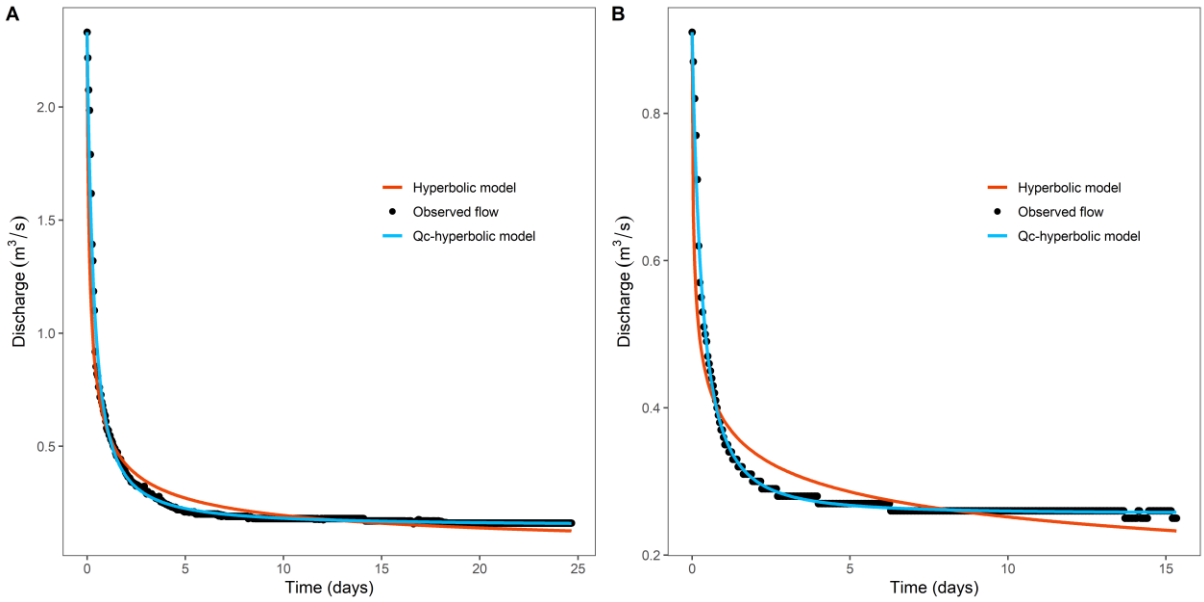

L Parameters in the Qc-hyperbolic model: *n* as a function of *α*.

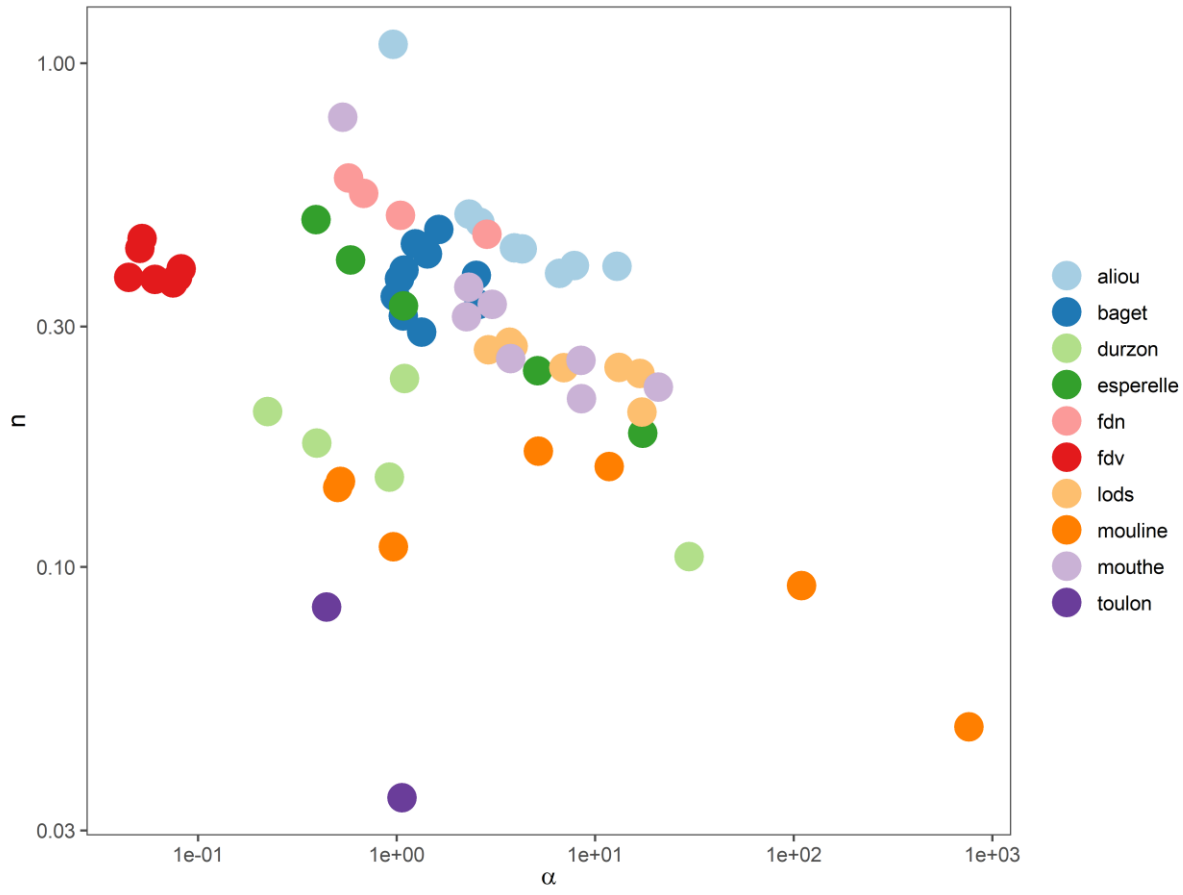

M All studied recessions simulated with the Qc-hyperbolic model. For each recession, the discharge was divided by the initial discharge to allow comparison among systems.

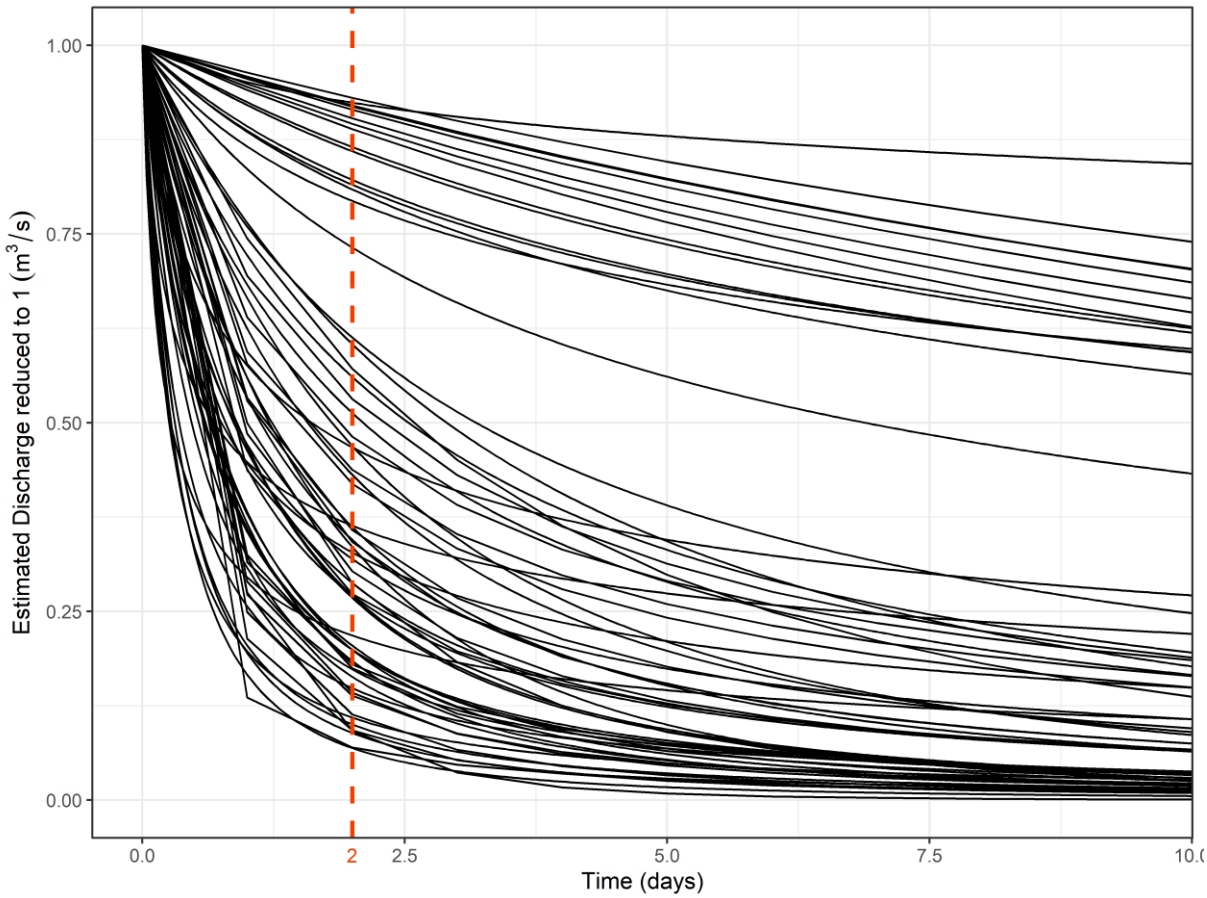

N Comparison of the results of (A) *h* and (B) *i*. (C) shows the correlation between the indicator from the Qc-hyperbolic model and the Mangin indicator.

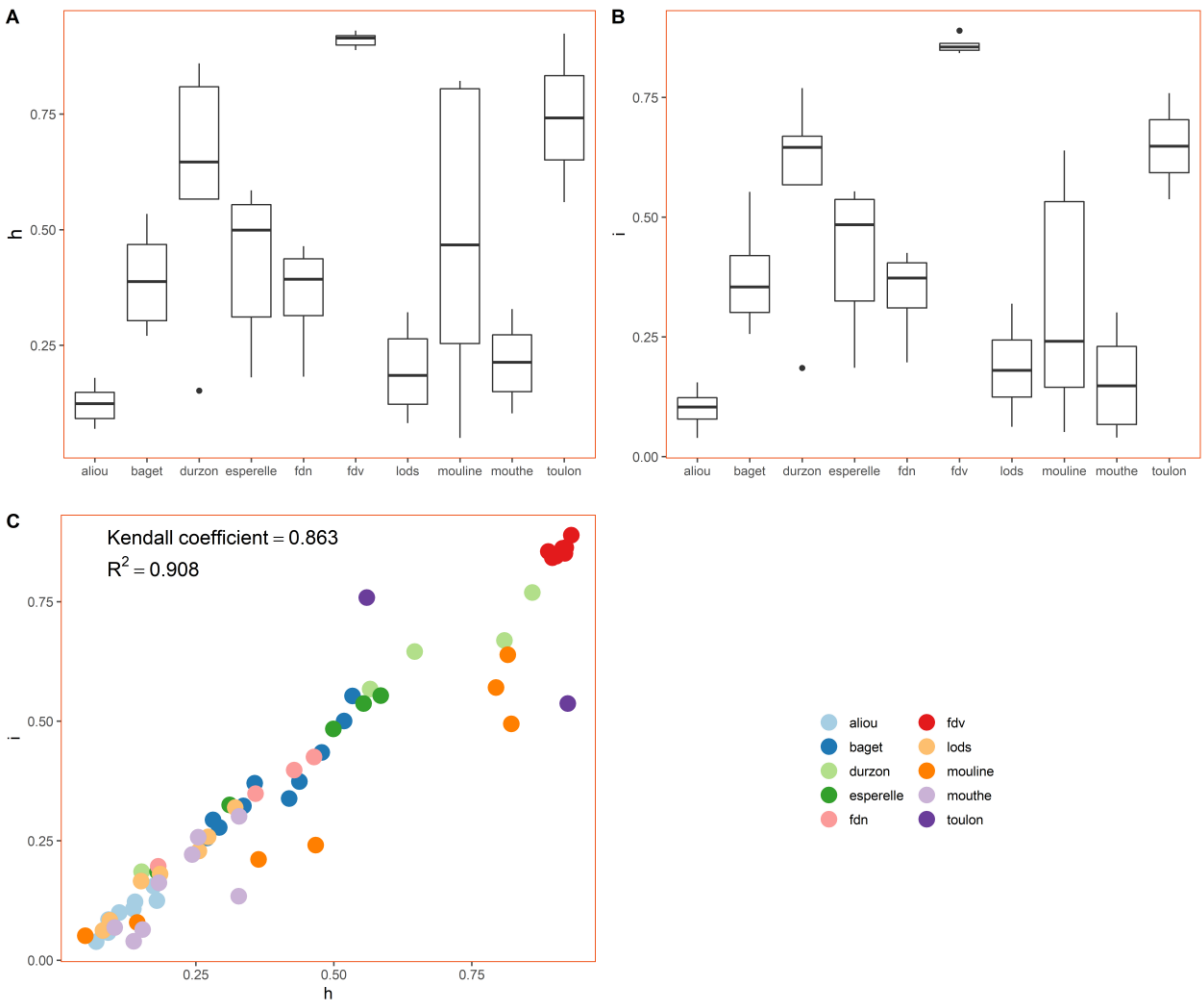

O Comparison of the results of (A) *k* and (C) discharge at the end of the recession limb divided by the mean interannual discharge, and (B) *i* and (D) discharge two days after the flood peak divided by the flood discharge. (E) and (F) show the correlation between statistical indicators and Mangin indicators.

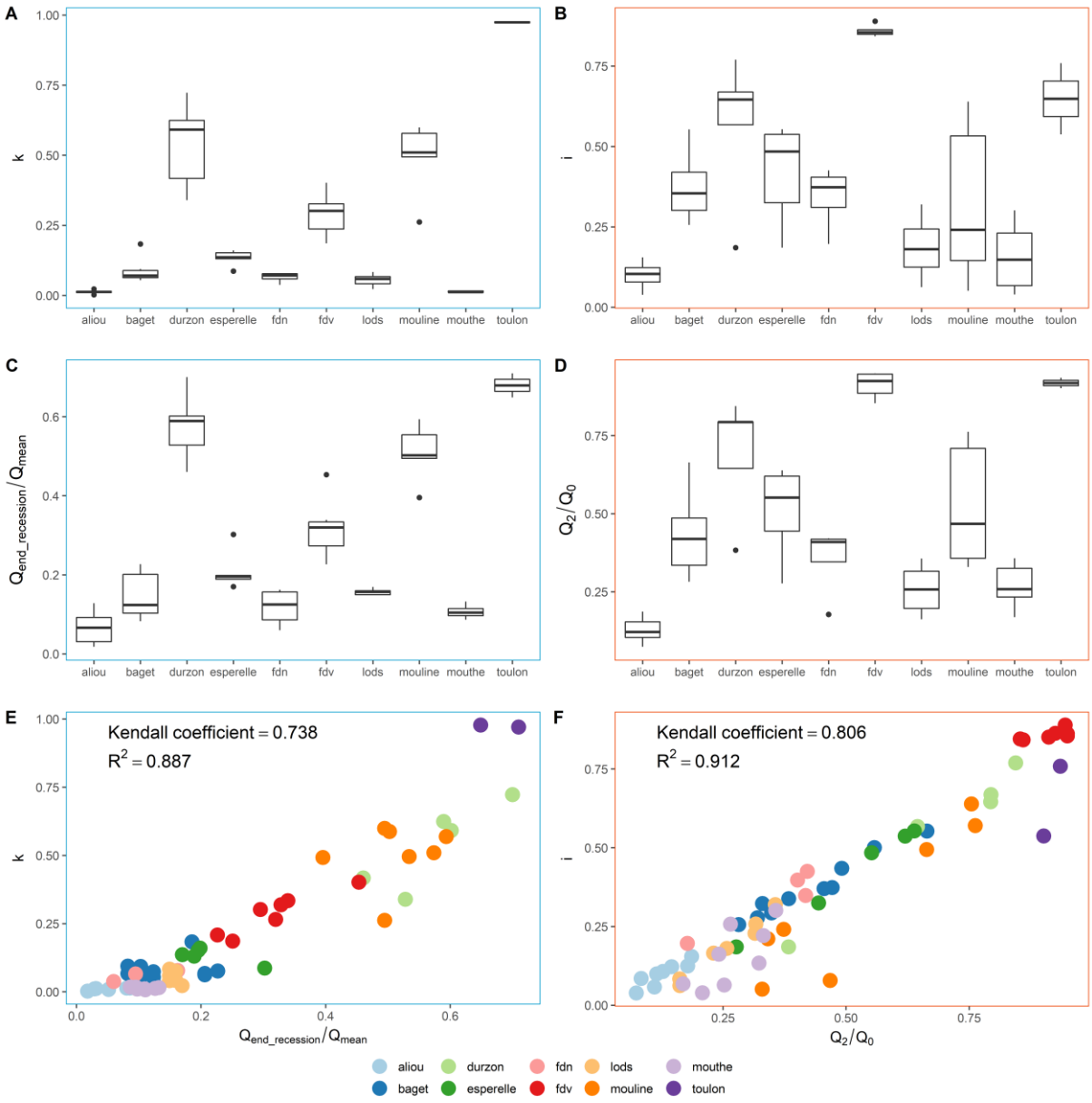

P Conductivity probability density function (*µS/cm*) for the studied systems.